Energy and Environmental Science, Volume 11, Issue 10, 2018, pp. 2647 - 2672
DOI: 10.1039/C8EE01393D

Enhanced hydrogen production from thermochemical processes - a review

Guozhao Ji,[a] Joseph G. Yao,[b] Peter T. Clough,[c] João C. Diniz da Costa,[d] Edward J. Anthony,[c] Paul S. Fennell,[b] Wei Wang,[a,e,f] and Ming Zhao[a,e,f,*]

a. School of Environment, Tsinghua University, Beijing 100084, China.
b. Department of Chemical Engineering, Imperial College London, South Kensington, London, SW7 2AZ, UK.
c. Energy and Power Engineering, Cranfield University, Cranfield, Bedfordshire MK43 0AL, UK.
d. FIM2Lab-Functional Interfacial Materials and Membranes Laboratory, School of Chemical Engineering, The University of Queensland, Brisbane, Qld, 4072, Australia.
e. Key Laboratory for Solid Waste Management and Environment Safety, Ministry of Education, Beijing 100084, China.
f. Beijing Engineering Research Center of Biogas Centralized Utilization, Beijing 100084, China.

To alleviate the pressing problem of greenhouse gas emissions, the development and deployment of sustainable energy technologies is necessary. One potentially viable approach for replacing fossil fuels is the development of a H_2 economy. Not only can H_2 be used to produce heat and electricity, it is also utilised in ammonia synthesis and hydrocracking. H_2 is traditionally generated from thermochemical processes such as steam reforming of hydrocarbons and the water-gas-shift (WGS) reaction. However, these processes suffer from low H_2 yields owing to their reversible nature. Removing H_2 with membranes and/or extracting CO_2 with solid sorbents *in situ* can overcome these issues by shifting the component equilibrium towards enhanced H_2 production *via* Le Chatelier's principle. This can potentially result in reduced energy consumption, smaller reactor sizes and, therefore, lower capital costs. In light of this, a significant amount of work has been conducted over the past few decades to refine these processes through the development of novel materials and complex models. Here, we critically review the most recent developments in these studies, identify possible research gaps, and offer recommendations for future research.

1. Introduction

There is currently a large concerted effort on the development of low-carbon and sustainable technologies to mitigate CO_2 emissions and combat climate change. This is evidenced by the recent Paris Agreement signed by 195 members of the United Nations Framework Convention on Climate Change (UNFCCC). Many strategies are now being considered to limit impacts of CO_2 emissions directly associated with the current carbon-based economy. One of these strategies is the deployment of H_2 as a clean energy vector. H_2 can play a vital role in the transition to a low-carbon economy, particularly in the energy, industry and transport sectors. H_2 is widely considered as an attractive energy carrier owing to its high calorific value by weight and its ability to effectively reroute CO_2 emissions to a point source ready for capture, transportation and storage (CCS).[1] Upon combustion, it does not emit CO_2 or other harmful gases, and can be stored safely (albeit not easily), and transported with existing technology.[2] In addition, H_2 is already widely used in many industrial applications including: fuel upgrading,[3] ammonia production,[4, 5] electricity production,[6, 7] heat generation,[8, 9] and for fuel cell applications.[10, 11] Ideal feedstocks for H_2 production include hydrogen-containing materials such as natural gas,[12] coal,[13, 14] glycerol,[15-21] alcohol,[22-27] petroleum oil,[28, 29] biomass,[1, 2, 30-36] chemicals[37-39] and industrial/municipal wastes.[38] H_2O is also a potential H_2 source if processed via electrolysis or reacted with other reactants such as coal or CO.[40-43] Although H_2 can be produced from a variety of sources, its yield is limited by the reversible nature of the thermochemical processes used to create it.[44] This often necessitates the use of nickel catalysts and reactors operating at elevated temperatures and pressures to improve reactant conversion.[45] Furthermore, the limited conversion of feedstock to H_2 is inevitably associated with the production of large quantities of unwanted by-products such as complex mixtures of condensable hydrocarbons and CO_2.[46] The removal of these by-products adds additional complexity and cost during the H_2 purification process. The most widely used methods to produce H_2 include steam reforming of methane (SMR)[47-51] and coal (or biomass to a lesser extent) gasification.[52-54] Coal and biomass gasification as described in Eqn. 1 require complex gas cleaning owing to the additional presence of volatiles, which may generate condensable vapours during gas separation, causing blockages and maintenance issues.

$$C_xH_yO_z \rightarrow \text{Volatiles} + \text{Tar} + \text{Char} \quad \Delta H^0_{298} > 0 \tag{1a}$$

$$\text{Tar} + \text{Char} + \text{Volatiles} + nH_2O \rightarrow H_2 + CO + CO_2 + CH_4 \quad \Delta H^0_{298} > 0 \tag{1b}$$

$$CH_4 + H_2O \leftrightarrow CO + 3H_2 \quad \Delta H^0_{298} = 206.2 \text{ kJ mol}^{-1} \tag{2}$$

$$CH_4 + 2H_2O \leftrightarrow CO_2 + 4H_2 \quad \Delta H^0_{298} = 165 \text{ kJ mol}^{-1} \tag{3}$$

In the case of steam reforming, H_2 purification involves mainly gas separation, as CH_4 is converted into CO, CO_2 and H_2 in the presence of steam according to Eqns. 2 and 3. Owing to the endothermic nature of these reactions, high CH_4 conversions can only be achieved at elevated operating temperatures (>727 °C).[45] However, a significant fraction of CO is also produced under these conditions. CO is a desirable product as it can be shifted with the addition of steam via water-gas-shift (WGS) reactors downstream of the reformer and, in doing so, produce more H_2; this is known as the WGS reaction.[48]

$$\mathrm{CO} + \mathrm{H_2O} \leftrightarrow \mathrm{CO_2} + \mathrm{H_2} \quad \Delta H^0_{298} = -41 \text{ kJ mol}^{-1} \tag{4}$$

Typically, industrial WGS reactors use a two-step shift to optimise H_2 yields and purity, and CO conversion. The first reactor is a high-temperature shift (300-450 °C) which possesses faster reaction kinetics but low CO conversion, followed by a low-temperature stage (175-250 °C) and high steam ratios to maximise CO conversion.[55, 56] Subsequently, there is a need to cool down the gas for downstream separation of the remaining gaseous impurities. Conventionally, the H_2 stream is finally purified with a pressure swing adsorption (PSA) train up to the desired purity, which can be as high as 99.99% for some applications.[57] The energy penalties for this configuration arise from the use of multiple high-temperature unit operations and cooling of intermediate streams.

Since the drawbacks of these processes are predominantly owing to the thermodynamic limitations of the reversible reactions, extensive research has been carried out to overcome these issues by purposely shifting the reaction towards the product side using Le Chatelier's principle.[58-63] The removal of either or both H_2 and CO_2 *in situ* results in enhanced H_2 production and reactant conversion. This can be achieved by employing H_2-selective membranes and/or using CO_2 sorbents. This review starts from the theoretical explanation of the shift effect and endeavours to highlight the development of membranes and sorbents for enhanced H_2 production from thermochemical processes. In addition, this work also covers studies which invoke computational fluid dynamic (CFD) simulations to gain better insight into these reaction processes to allow optimisation of operating conditions and reaction design.

2. Mechanism of the shift effect

2.1 Reaction rates

Several reaction rate models have been proposed for modelling the kinetics of SMR and WGS over the past years.[34, 42, 64-66] Xu and Froment[67] have systematically tested SMR kinetics in the presence of a Ni/Al_2O_3 catalyst and developed a general form of the SMR and WGS reaction rates based on a Langmuir-Hinshelwood Hougen-Watson (LHHW) mechanism (Eqns. 5-7). This model has since been adopted by many researchers.[68-70]

$$r_1 = \frac{k_1}{p_{\mathrm{H_2}}^{2.5}} \frac{\left(p_{\mathrm{CH_4}} p_{\mathrm{H_2O}} - \frac{p_{\mathrm{H_2}}^3 p_{\mathrm{CO}}}{K_1} \right)}{DEN^2} \tag{5}$$

$$r_2 = \frac{k_2}{p_{\mathrm{H_2}}^{3.5}} \frac{\left(p_{\mathrm{CH_4}} p_{\mathrm{H_2O}}^2 - \frac{p_{\mathrm{H_2}}^4 p_{\mathrm{CO_2}}}{K_2} \right)}{DEN^2} \tag{6}$$

$$r_3 = \frac{k_3}{p_{\mathrm{H_2}}} \frac{\left(p_{\mathrm{CO}} p_{\mathrm{H_2O}} - \frac{p_{\mathrm{H_2}} p_{\mathrm{CO_2}}}{K_3} \right)}{DEN^2} \tag{7}$$

$$DEN = 1 + K_{\mathrm{CO}} p_{\mathrm{CO}} + K_{\mathrm{H_2}} p_{\mathrm{H_2}} + K_{\mathrm{CH_4}} p_{\mathrm{CH_4}} + K_{\mathrm{H_2O}} \frac{p_{\mathrm{H_2O}}}{p_{\mathrm{H_2}}} \tag{8}$$

Here, $\frac{k_1}{p_{\mathrm{H_2}}^{2.5}}$, $\frac{k_2}{p_{\mathrm{H_2}}^{3.5}}$ and $\frac{k_3}{p_{\mathrm{H_2}}}$ are kinetic factors, $p_{\mathrm{CH_4}} p_{\mathrm{H_2O}} - \frac{p_{\mathrm{H_2}}^3 p_{\mathrm{CO}}}{K_1}$, $p_{\mathrm{CH_4}} p_{\mathrm{H_2O}}^2 - \frac{p_{\mathrm{H_2}}^4 p_{\mathrm{CO_2}}}{K_2}$ and $p_{\mathrm{CO}} p_{\mathrm{H_2O}} - \frac{p_{\mathrm{H_2}} p_{\mathrm{CO_2}}}{K_3}$ are reaction driving forces, and DEN^2 is the adsorption expression.

It is clear from these equations that the forward reaction for H_2 production increases when there is a reduction in the partial pressures of the product components. Decreasing p_{H_2} and p_{CO} enhances the driving force of reaction (4) and decreasing p_{H_2} and p_{CO_2} improves the driving force of reactions (3) and (4).

2.2 Shifting reactions

Primary techniques for *in situ* product removal of H_2 or CO_2 in these equilibrium-limited reactions include: permeating H_2 through selective membranes[71-73] or capturing CO_2 with solid sorbents[21, 74] *via* the sorption-enhanced reforming (SER) process. In both cases, the reactions (see WGS reaction as an example) tend to be equilibrium-limited, meaning the production of H_2 and CO_2 are limited by gas concentrations and operating conditions. For H_2-selective membranes, the H_2 permeation through the membrane can be calculated with Eqn. 9.

$$Q_{H_2} = \left(\frac{P}{l}\right)\left(xp_f - yp_p\right)\cdot A \tag{9}$$

where Q_{H_2} is the H_2 permeation flow rate, $\left(\frac{P}{l}\right)$ is the permeance of H_2 through this membrane, p_f is the feed pressure, p_p is the permeate pressure, x is the H_2 fraction in feed gas, y is the H_2 fraction in permeate gas and A is the membrane area.

The permeation of H_2 reduces its partial pressure in the reactor and then increases the driving force terms of Eqns. 5-7. In the case of membrane reactors under steady state conditions, the membrane will facilitate the removal of H_2 that is being generated in the reaction chamber. In this case, the total pressure and partial pressure of gases in the membrane reactor remain constant. There are two important engineering parameters which need to be balanced, namely: the Damköhler number (*Da)* and the Péclet number (*Pe)*. Da relates the reaction rate to the feedstock rate and Pe is associated with the hydrogen permeation rate to the ideal hydrogen generation rate as follows:

$$Da = \frac{rV}{F} \tag{10}$$

$$Pe = \frac{nF}{Q_{H_2} A} \tag{11}$$

where r is the feedstock reaction rate, F is the feedstock flow rate and n is the stoichiometry number of hydrogen produced per mole of feedstock. The product $DaPe$ provides a measure of the effectiveness of a membrane reactor. If $DaPe$ = 1, all hydrogen generated is removed, whereas $DaPe$ < 1 implies the reactor throughput could be enhanced, and $DaPe$ > 1 indicates membrane area is insufficient to remove all the generated hydrogen.[38]

Another way to enhance the hydrogen purity and influence the equilibrium position of the system is through SER. The rate of CO_2 removal in this process can be expressed by Eqn. 12.[75, 76]

$$\frac{dC_{CO_2}}{dt} = -kC_{CO_2}(1-\alpha) \tag{12}$$

Here, α is the sorbent conversion, C_{CO_2} is the CO_2 concentration and k is the rate constant for sorption. By decreasing the CO_2 partial pressure in the sorption-enhanced reactor, an increase in the driving force terms of Eqns. 5-7 will lead to greater H_2 production.

By employing both membranes and CO_2 sorbents in the same reactor, it is possible to further enhance the driving force. Hence, an even better shift effect would be expected.

3. Shift effect by membrane permeation

Membrane separation is attractive in H_2 production technology, as it can be operated in a continuous manner. Feeding of reactant gases (such as CH_4, CO and H_2O) and removal of separated gas can occur simultaneously, due to the membrane acting as a selective, permeable reactor wall for the gases. The H_2-selective membrane allows H_2 to permeate out of the reactor while keeping other gases in the reactor. A H_2 membrane reactor for assisting SMR is illustrated in Fig. 1. Here, CH_4 and H_2O are fed into the membrane reactor, and react to form H_2 and CO_2 via SMR/WGS (Eqns. 2-4). The removal of H_2 shifts the system equilibrium (Fig. 1), making it possible to achieve a lower H_2 partial pressures within the reactor itself relative to that of a traditional SMR reactor. This, in turn, allows higher CH_4 conversions to be obtained.

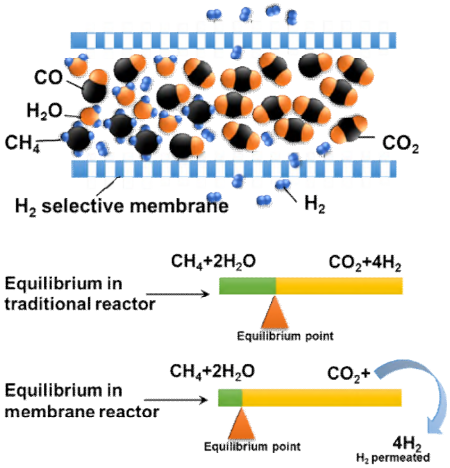

Fig. 1. Schematic of system equilibrium shift during SMR (Eqn. 3) due to the application of a H_2-selective membrane.

A good H_2 membrane should have high permeability (gas quantity permeated per unit area under unit pressure gradient) and selectivity (permeability of one gas preferentially over another gas) towards H_2. A high selectivity towards H_2 is desired as this avoids the need of an extra purification step downstream. Since H_2 production (Eqns. 1-4) typically requires high operating temperatures, it is imperative to develop membranes with excellent thermal stability.[77] This means that most commercially-available membranes (especially polymeric membranes) and newly-developed metal organic framework (MOF) membranes are not suitable for this application owing to their high organic content.[78] Consequently, most of the research in this field has sought to develop inorganic membranes.[79-86] Suitable membranes should also demonstrate good hydrothermal and chemical resistance in order to handle high-temperature steam and poisonous trace gases such as CO and H_2S.

3.1 Palladium-based membrane reactors

Materials containing elements from group 10 of the periodic table such as Ni, Pd, and Pt are able to dissociate and dissolve hydrogen.[87] Pd, in particular, has demonstrated a superior ability to permeate hydrogen relative to the other elements in its group. This is due to Pd having a much higher solubility of hydrogen, over a wide temperature range.[87] Consequently, Pd has been identified as a membrane material with great potential. As illustrated in Fig. 2, H_2 molecules first dissociate into H atoms upon contacting the the Pd membrane surface on the feed side. The atomic H then diffuses to the permeate side of the membrane through a partial pressure gradient. This is followed by association and desorption of the H_2 molecules at the permeate side. The lattice constant of Pd is 389 pm,[88] and the Pd atom radius is 139 pm.[89] This leaves an interstitial gap of 111 pm which only allows H atoms, which have a diameter of 62 pm,[89] through. The other gases (CO_2, CO, H_2O and CH_4) are simply too large since the C and O atoms have a diameter of 152 pm[89] and 132 pm,[89] respectively. This gives Pd perfect selectivity for H_2. The permeate flux of H_2 across a Pd membrane is generally governed by Sieverts' law (Eqn. 13).[90-94]

$$J_{H_2} = \left(\frac{P_m}{l}\right)\left(\sqrt{p_{H_2,feed}} - \sqrt{p_{H_2,permeate}}\right) \quad (13)$$

where P_m is the permeability, l is the membrane thickness, $P_{H_2,feed}$ is the H_2 pressure at the feed side, and $P_{H_2,permeate}$ is the H_2 pressure at the permeate side.

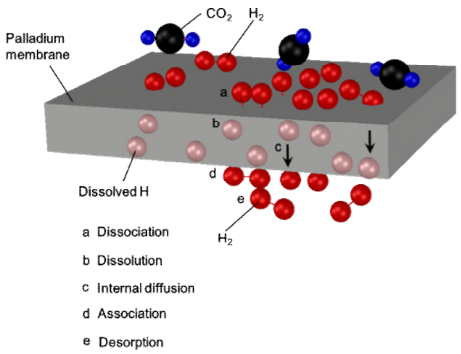

Fig. 2. Schematic of palladium membrane separation mechanism.

Pd membranes are generally extremely thin (a few hundred nanometres to a few microns in thickness),[50, 95-97] and possess superior solubility of hydrogen over other materials.[5, 87] This combination of properties results in very good permeability.[87] Besides high selectivity and permeability, Pd membranes are also able to withstand high temperatures (up to 714 °C).[98] In view of these qualities, the Pd-based membrane has been the most intensively investigated membrane for enhancing H_2 generation over the past several decades.[12, 27, 50, 87, 99-106]

One major challenge of using Pd membranes for H_2 separation is that Pd undergoes phase transformation (α↔β) from a low H/Pd atomic ratio to a high H/Pd atomic ratio when the temperature is below its critical point (298 °C).[87] The difference in lattice parameter (0.3895 nm for the α phase and 0.410 nm for the β phase) causes distortions which can lead to cracks, defects or pinholes in the film.[107] With the purpose of preventing phase transition and relieving embrittlement, palladium is often alloyed with other metals such as Ag,[107-109] Cu,[110-114] Au[115] or Ru.[51, 116-118] Alloying was found to reduce the critical temperature for the α↔β phase transition.[87] As well as having greater resistance to phase transitions, some binary palladium alloys have demonstrated improved H_2 permeation.[90, 113, 116, 119] The enlarged atomic bond distance due to the presence of the other metal was found to facilitate atomic H diffusion. Extensive experimental work as well as density functional theory (DFT) calculations have also demonstrated that Pd-based alloy membranes are able to enhance H_2 permeation.[112, 113, 120, 121] In view of the success of alloyed Pd membranes in promoting permeation and preventing phase transition, they have also been deployed for enhancing H_2 production.[51, 94, 114, 117, 122-125]

Table 1 summarises studies which have employed Pd-based membranes to enhance H_2 production via thermochemical conversions. The obtained H_2 purity is omitted in Table 1, since they are all close to 100% (>97%,[126] >99.8%,[119] >99.9%,[27] >99.9999%,[111] 100%[124, 127]) owing to the high H_2 selectivity of Pd-based membranes. Since the feedstock conversion to H_2 is a function of pressure, temperature, steam-to-carbon (*S/C*) ratio, space velocity and catalyst activity, it is difficult to make a direct comparison between experiments to judge their performance. The feedstock conversion generally increases with temperature and *S/C* ratio, but decreases with pressure and space velocity. Fig. 3 shows a comparison between the equilibrium conversion of CH_4 based on the work by Hou *et al*.[128] *vs.* experimental work[49, 117, 124, 129-131] invoking Pd membranes to enhance H_2 production for a range of temperatures, pressures and *S/C*. The head of the stems in Fig. 3 marks the maximum CH_4 conversions. It can be seen that significantly higher CH_4 conversions can be reached relative to conventional SMR for the same set of operating conditions.

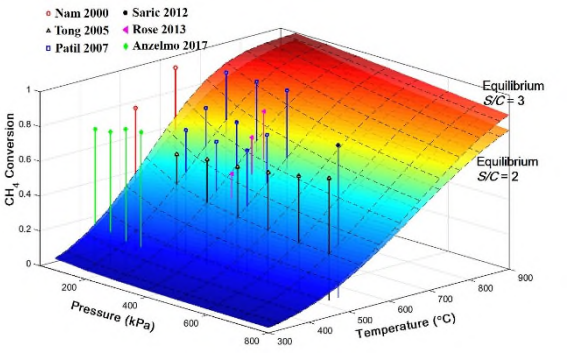

Fig. 3. The comparison of enhanced CH_4 conversion by employing palladium-based membrane to CH_4 conversion at thermodynamic equilibrium in SMR. (Data were extracted from Nam *et al.*,[117] Tong *et al.*,[129] Patil *et al.*,[49] Saric *et al.*,[130] Rose *et al.*,[131] and Anzelmo *et al.*[124])

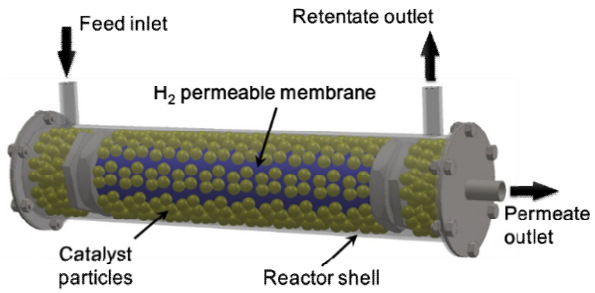

Fig. 4. Configuration of a fixed-bed membrane reactor.

Table 1 Operating conditions and performance of Pd-based membrane reactors for reforming carbon monoxide, methane, methanol and ethanol.

Feedstock	Membrane	ΔPressure (kPa)	Temperature (ºC)	Catalyst	*S/C* ratio[a]	Space velocity (h^{-1})	Conversion (%)	Reference
CO	Pd	1378	349	Fe-Cr oxide	1.4	860	99	100
CO	Pd	1100	350	$Pt/Ce_{0.6}Zr_{0.4}O_2$	3	4050[b]	96.5	132
CO	Pd	0[c]	400	Iron based	3	611[b]	~92	101
CO	Pd	300	400	Fe-Cr oxide	1	5000	65	133
CH_4	Pd-Ru	250	500	Ni	3	837	77.5	51
CH_4	Pd/PSS	200	400	Ni	3.5	2600	84	124
CH_4	Pd-Ag-V-Ni	0[c]	500	Ni/SiO_2	2	1467[b]	60	134
CH_4	Pd-Ag	1000	525	Pt_3Ni_{10}/CeO_2	3	136	90	135
CH_4	Pd	300	500	Ni	3	1120	~98.6	136
CH_4	Pd	300	500	Ni	3	2240	~79.3	136
CH_4	Pd	300	600	Ni	3	2240	~90	136
CH_4	Pd	300	550	Ni/Al_2O_3	3	~550	~100	137
CH_4	Pd	300	527	Ni	3	1120	~97	129
CH_4	Pd-Ru	0[c]	500	Ni	3	92[b]	80	117
CH_4	Pd/Al_2O_3	2735	580	Ni	3	760[b]	98	130
CH_4	Pd	800	550	Ni	3	3000	68	138
CH_4	Pd	1600	650	Ni	3	600	60	50
CH_4	Pd-Ru	2900	580	Ni	3	150	85	118
CH_4	Pd-Au	2800	511	Ru	3	147	94	115
CH_4	Pd/PSS	100	500	Ru	2	187[b]	86	139
CH_4	Pd/Al_2O_3	100	500	Ni	3	692[b]	76	106
CH_4	Pd-Ag	100	500	Ni	3	224[b]	51	108
CH_4	Pd-Ag	120	450	Ni	3	141[b]	60	140
CH_4	Pd/Al_2O_3	90	550	NiO	3	3994[b]	99	12
CH_4	Pd-Alloy	90	540	Ni	3~3.2	800	80	141
CH_4	Pd-Ag	130	600	$Ru/Ce_{0.75}Zr_{0.25}O_2$	3	-	96.7	94
CH_4	Pd-Ag	300	600	$Ni/CaAl_2O_3$	3	-	82	142
CH_4	Pd-Ag	350	630	Noble metal	3	364[b]	83.1	131
CH_4	Pd-Ag	900	550	-	3	-	73.1	58

CH_4	Pd-Ag	100	600	Ni/Al_2O_3	-	2988[b]	60	143
CH_3OH	Pd-Ag	250	280	$Cu-Zn/Al_2O_3$	3	1800	100	109
CH_3OH	Pd	1418	350	$Cu/ZnO/Al_2O_3$	1.2	1[d]	95	27
CH_3OH	Pd	250	330	Cu-Zn	2.5	18500	85	144
CH_3OH	Pd	150	300	CuO/ZnO	1.5	665[b]	97	145
CH_3OH	Pd-Ag	100	400	Cu-Zn/GaOx	2	111[b]	88	146
CH_3OH	Pd	246	300	$Ni-Zn/Al_2O_3$	1	17.53[d]	80	147
C_2H_5OH	Pd-Ag	0[c]	500	Rh/CeO_2	5	-	100	148
C_2H_5OH	Pd-Ag	1400	350	$Co[Si_2O_5](OH)_2$	3	4.6[d]	100	149
C_2H_5OH	Pd-Ag	150	400	Co/Al_2O_3	9.35	5.5[b]	~95	150
C_2H_5OH	Pd-Ag	300	400	Co/Al_2O_3	9.35	4.59[b]	100	151
C_2H_5OH	Pd-Ag	1200	600	Co hydrotalcite	1.5	-	100	60
C_2H_5OH	Pd	1200	400	Co/Al_2O_3	2	9.94[d]	94	152
C_2H_5OH	Pd	500	340	$Pt-Ni/CeO_2$	1.5	0.3[d]	100	153
C_2H_5OH	Pd	300	400	Ni/CeO_2	6.5	5000	98	154
C_2H_5OH	Pd-Cu	100	352	Na-Co/ZnO	1.5	4400	62	105
C_2H_5OH	Pd	100	360	Na-Co/ZnO	6.5	9800	74	114
C_2H_5OH	Pd-Ag	1100	400	$Pd-Rh/CeO_2$	3	800	94	155
C_2H_5OH	Pd-Ag	1200	600	$Pd-Rh/CeO_2$	1.6	60–150	100	156
C_2H_5OH	Pd-Ru	-	550	Pt-Ru	4.5	-	99	157

[a] *S/C* ratio, Steam to carbon ratio
[b] GHSV, Gas hourly space velocity ($\times 10^3$ cm^3 h^{-1} $kg\text{-}cat^{-1}$)[158]
[c] Sweep gas was used to generate H_2 pressure difference
[d] WHSV, weight hourly space velocity (h^{-1})

A fixed bed (sometimes referred to as packed bed) is the most popular configuration for palladium membrane reactors due to its simplicity (Fig. 4).[102, 133, 135, 149, 152-154, 159] Furthermore, the immobility of the solid catalysts in this setup avoids damage and erosion to the delicate membrane layer.[160] The reactant gases are fed through the inlet and are passed over a catalytic bed where SMR takes place. The generated H_2 then permeates across the membrane and is collected from the permeate outlet stream. The other gases exit the reactor *via* the retentate outlet. This configuration has been applied in several studies to convert CH_4 to H_2.[12, 129, 136, 137, 139] The CH_4 conversions have been reported to be ~270%,[12] ~244%,[139] ~249%,[138] and ~405%[118] higher than those obtained in conventional reactors under identical operating conditions. Other than the tubular-shaped membrane depicted in Fig. 4, disk-shaped membranes have also been employed. Matsuka *et al*.[134] studied membrane-assisted SMR (MASMR) in a disk-shaped membrane reactor; however, they reported only a 55% improvement in CH_4 conversion relative to conventional SMR. This was due to the disk-shaped membranes having a lower membrane area-to-reactor size ratio compared to the tubular reactors. Since the shift effect is directly related to the H_2 permeation flow per unit reactor volume, a straightforward approach to promote the enhancement is to intensify the degree of H_2 permeation. Tong *et al.*[136] demonstrated that under identical operating conditions (*S/C* = 3, *T* = 500 or 550 °C) the CH_4 conversions in a more-permeable membrane reactor were always higher than those in the less-permeable reactor. Unfortunately, improving membrane permeability is technically challenging.[161] Instead, the permeate flux can be improved by magnifying the permeation driving force. This can be achieved by using a sweep gas (generally Ar[101, 124] and N_2[135, 136, 139, 148]) on the permeate side to maintain a high H_2 pressure gradient between the two sides of the membrane. However, the use of sweep gas is not desirable, as the purified H_2 is mixed with another gas, therefore, defeating the purpose of using membranes for gas separation. Using steam as a sweep gas[93,162] is a feasible approach, as steam can be condensed downstream of the membrane and easily separated from H_2. However, generation of steam accompanied by a condensation step may be prohibitive due to high energy consumption.

Aside from reactor configuration, the effects of system pressure in membrane reactors have also been investigated. Although high pressures drive the unfavourable methanation reaction which reduces the overall CH_4 conversion, it can also help facilitate H_2 permeation. Tong *et al*.[136] observed an increase in CH_4 conversion with pressure (1×10^5~3×10^5 Pa at

500 and 550 °C) in a Pd membrane reactor. Kim *et al*.[51] also found the CH_4 conversion increased with pressure in a Pd-Ru membrane reactor (2×10^5~3.5×10^5 Pa at 500 °C). Abu *et al*.[118] used a Pd-Ru membrane for SMR and noticed rising CH_4 conversion with pressure (0.7×10^5~3.2×10^5 Pa with *S/C* = 3 at 580 °C). This suggests that the overall effect of pressure is positive, at least under these particular conditions.

The use of fixed-bed reactors often warrants criticism because of their poor mass and heat transfer efficiency associated with the existence of temperature and concentration boundary layers.[163] The excessive pressure drop in packed-bed reactors can to some extent be circumvented by pelletising catalyst powders into larger particles. This seriously compromises the contactable surface area for reactant gases and reduces the effective catalyst activity by ~2-3 orders of magnitude.[163, 164] To overcome these limitations, fluidised-bed membrane reactors were proposed because of improvements in heat and mass transfer properties (Fig. 5).[165, 166] An early study of fluidised Pd membrane reactors was carried out by Adris *et al*.[165, 166] who developed an experimentally-validated model to analyse the effect of operating parameters such as pressure, temperature, *S/C* ratio, feed flow rate and sweep flow rate. Chen *et al*.[167] compared the performance of fluidised- and fixed-bed membrane reactors utilising a mathematical model, and predicted that higher CH_4 and H_2O conversions and H_2 yield should be obtained with the fluidised membrane reactor. The models of Adris *et al*.[165] and Chen *et al*.[167] were used to determine the gas flow rate and temperature profiles as a function of the reactor length. The model predicted a uniform temperature distribution owing to the homogeneous mixing of turbulent gases and particles in the fluidised bed. Due to the advantage in mass and heat transfer, a number of experimental demonstrations have employed Pd-based fluidised membrane reactors to produce H_2 from CH_4.[49, 58, 131, 142, 168] The catalyst activity can also be improved since fluidised bed reactors can utilise smaller particles (85-90 μm,[168] 50-75 μm,[49] 90 μm,[58] and 150-250 μm[142]).

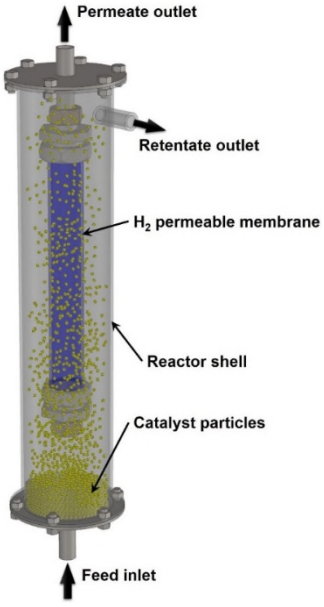

Fig. 5. Configuration of fluidised-bed membrane reactor.

Despite these attractive properties, there are also a number of weaknesses associated with fluidised-bed membrane reactors. For instance, the fluidised particles may damage the membrane surface and result in diminished separation efficiency. Coating the selective membrane layer on the permeate side could expose the substrate side to the catalyst and avoid attrition. However, this arrangement increases the risk of membrane delamination owing to the pressure difference between the reaction and permeate sides.[160] In addition, high gas velocities are required to fluidise the solids. This often leads to low residence time and, therefore, low reactant conversion and H_2 recovery.[142]

Besides methane, which is the most studied light hydrocarbon for H_2 production, there are also a number of studies using methanol and ethanol as the feedstock (Table 1). These alcohols are steam reformed in H_2 according to Eqns. 14 and 15.

$$CH_3OH + H_2O \leftrightarrow CO_2 + 3H_2 \quad \Delta H^0_{298} = 49.5 \text{ kJ mol}^{-1} \tag{14}$$

$$C_2H_5OH + 3H_2O \leftrightarrow 2CO_2 + 6H_2 \quad \Delta H^0_{298} = 347.4 \text{ kJ mol}^{-1} \tag{15}$$

Methanol steam reforming normally takes place at relatively low temperatures (280-400 °C[144, 145, 169, 170]) since it does not possess carbon-carbon bonds, which are difficult to break.[171] Lin *et al.*[27] conducted methanol steam reforming in both a conventional reactor and a Pd membrane reactor. In the conventional reactor, the methanol conversion was found to reach >90% at 350 °C, while >95% conversion was achieved with the aid of a Pd membrane. Lin *et al.*[27] also demonstrated that the Pd membrane could handle 900 h of continuous operation without any noticeable reduction in the H_2 yield and methanol conversion, mostly due to the mild operating temperatures that are required for methanol steam reforming. By employing a Pd-Ag membrane, Ghasemzadeh *et al.*[109] improved the methanol conversion to 100% at 280 °C which is at the lower end of current standard operating temperatures.

Ethanol, on the other hand, needs relatively high temperatures to reform owing to its greater enthalpy reaction (Eqn. 15).[160] Through the work conducted by Deluga *et al.*[172] it was indicated that an operating temperature of at least 700 °C is needed to achieve full conversion when a membrane is not present. Hedayati *et al.*[156] reduced the required temperature for full conversion to 600 °C by employing a Pd-Ag membrane (*S/C* = 1.6~3). Iulianelli *et al.*,[150, 151] who also used a Pd-Ag membrane, achieved almost full conversion of ethanol at 400 °C by using a higher steam-to-carbon ratio (*S/C* = 9.35; H_2O/C_2H_5OH = 18.7/1 (mol/mol)).

Despite the promising results from enhancing H_2 production with Pd membranes, there are still a few barriers to commercial deployment. The first evident disadvantage is the high cost of palladium and its alloys. The price of the most common palladium precursor, $PdCl_2$, is around 100 US$$_{2017}$/g. Coating ultra-thin membranes (a few hundred nanometres) would reduce the quantity of palladium material required, and improve the H_2 permeation, but the trade-off is that the low thickness of the membrane may increase the risk of membrane defects and pinholes, resulting in poor H_2 selectivity. Secondly, the exposure to CO and H_2S in the reactant gas could deactivate the surface of the membrane. The adsorption of CO and H_2S molecules can block the pathway for H_2 and inhibit its permeation.[173] Another issue is pointed out by Eqn. 13, in which H_2 permeation is proportional to the difference of the square root of the pressure drop across the membrane. Therefore, enhancing the permeation by compressing feed gas is not as efficient compared to permeation mechanisms in which the permeation is proportional to pressure.

3.2 Silica-based membrane reactors

Silica membranes are a promising alternative to Pd membranes. Silica is abundant, inexpensive, and is not affected by CO poisoning.[97] As an inorganic material, silica also displays excellent long-term thermal stability at high temperatures.[174] Amorphous silica can be derived from precursors such as tetraethoxysilane (TEOS),[175] tetramethoxysilane (TMOS),[176] dimethoxydiphenylsilane (DMDPS),[177] Ethoxy Polysiloxane (ES40)[80] and hexamethyldisiloxane (HMDS),[45] and can form a microporous structure.[84, 178] As shown in Fig. 6, silica with micropores of a suitable size (*i.e.*, between the H_2 kinetic diameter (0.29 nm) and other gases' kinetic diameters (CH_4: 0.38 nm; CO: 0.37 nm; CO_2: 0.34 nm))[179] can act as molecular sieve for H_2 separation. Gas permeation flux across silica-based membranes is generally expressed by the activated transport model (Eqn. 16).[84]

$$J = \left(\frac{P_0}{l}\right)\exp\left(-\frac{E_a}{RT}\right)\Delta p \tag{16}$$

Here, (P_0/l) is the pre-exponential permeance and E_a is the apparent activation energy. The apparent activation energy is positive for H_2 permeating through a silica membrane, but generally negative for larger molecules such as CO_2, CO or CH_4.[82, 174, 180, 181] The signs of the activation energies of H_2 and other gases not only increases H_2 permeation flux at elevated temperatures but also amplifies the selectivity of H_2 over other gases, ensuring a high purity of H_2 in the permeate stream.[181, 182]

An early attempt at using silica material as a H_2 membrane reactor was for comparison with a Pd-Ru membrane for MASMR.[117] The silica membrane reactor was found to be less effective at enhancing CH_4 conversion since H_2 permeation through the silica membrane was an order of magnitude lower than that of Pd-Ru membrane under low-pressure conditions (1.01325×10^5 Pa). Tsuru *et al.*[183] prepared TEOS-derived silica membranes for MASMR at 500 °C at 1 bar with *S/C* = 3. An increase in CH_4 conversion to approximately 80% (from the equilibrium conversion of 44% for a traditional reactor) was reported. Two silica membrane reactors made from TMOS and HMDS precursors by Akamatsu *et al.*[45] via the chemical vapour deposition (CVD) method were also tested for SMR with *S/C* = 3 at 500 °C. Both silica membrane reactors enhanced CH_4 conversion from ~44% to ~90% at 1.0×10^5 Pa. Tsuru *et al.*[184] prepared Ni-doped silica membranes from $Ni(NO_3)_2$ and TEOS precursors; the SMR tests at 500 °C showed that the derived silica membrane increased the conversion from 30% to 80% at 4.0×10^5 Pa and pure H_2 was produced.

In addition to methane reforming, silica membranes were also used to enhance the H_2 yield from a number of other thermochemical reactions. Silica-based membranes are more popular than Pd-based membranes for enhancing the WGS reaction because they are not as susceptible to CO poisoning.[103, 185] Giessler *et al.*[186] employed a hydrophobic silica membrane and a hydrophilic membrane reactor for membrane-assisted water-gas-shift (MAWGS). Although the

conversion of CO (~95%) was found to improve at temperatures above 250 °C in the presence of both membranes, the CO conversion was found to fall below the equilibrium levels for unassisted WGS at the lower range of temperatures. The low conversion was potentially due to diminished H_2 permeation at low temperatures. Secondly, the reaction kinetic factor was very low so very long residence times were required.[187, 188] Brunetti *et al.*[187, 189] tested flat sheet silica membranes for MAWGS between 220-290 °C and found the CO conversion exceeded conventional equilibrium conversion at temperatures >250 °C. The authors also reported that elevated pressures improved CO conversion, most likely owing to improved permeation, since pressure does not affect the equilibrium position of the WGS reaction owing to equimolar stoichiometry of the reactant and products. Table 2 summarises an up-to-date list of experimental studies on the use of silica as a membrane reactor for enhanced H_2 production. Several representative experimental results are plotted in Fig. 7. It can be seen that the CO conversions were improved relative to conventional WGS but the degree of enhancement is not as significant as for the improvement of CH_4 conversion with Pd membranes (Fig. 3). This is because WGS is usually carried out at lower temperatures compared to SMR due to the exothermicity of WGS and, therefore, exhibits slower kinetics at lower temperatures. [190]

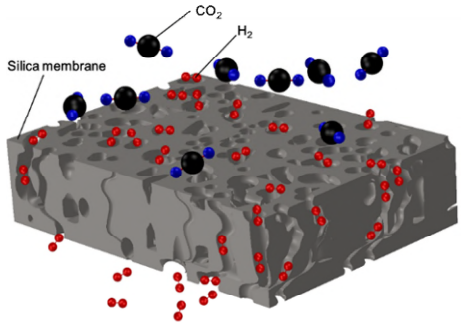

Fig. 6. Schematic of silica membrane separation mechanism.

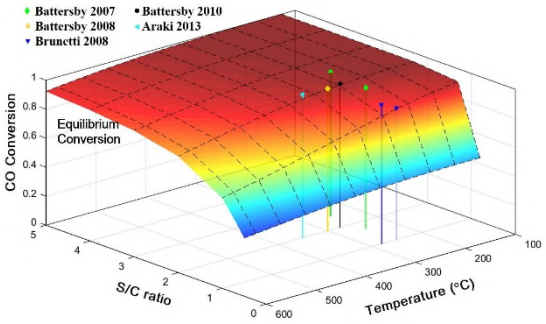

Fig. 7 The comparison of enhanced CO conversion by employing silica-based membrane to CO conversion at thermodynamic equilibrium in water-gas-shift reaction. (Data were extracted from Battersby *et al.*,[191] Battersby *et al.*,[188] Brunetti *et al.*,[189] Battersby *et al.*,[192] and Araki *et al.*[190])

Table 2. Operating conditions and performance of Si-based membrane reactors for H_2 production *via* thermochemical conversions.

Feedstock	Membrane	ΔPressure (kPa)	Temperature (°C)	Catalyst	*S/C* ratio[a]	Space velocity (h^{-1})	Conversion (%)	H_2 purity (%)	Reference
NH_3	POSS-silica	100	450	Ru/Al_2O_3	-	95.54	74	84	[193]
NH_3	POSS-silica	100	450	Ru/Al_2O_3	-	11.3	95	89	[194]
CO	Silica	-	260	Cu–Zn	3	0.612[b]	~95	~88	[195]
CO	Silica	400	275	$Cu\text{-}ZnO/Al_2O_3$	1	2652	~73		[196]
CO	Silica	200	350	Pt	2	1800[c]	~99	99.7	190
CO	Cobalt silica	400	300	$Cu\text{-}ZnO/Al_2O_3$	2	-	98	85	[192]
CO	Cobalt silica	400	500	Fe_3O_4/Cr_2O_3	2	-	90	-	[192]
CO	Cobalt silica	200	300	$Cu\text{-}ZnO/Al_2O_3$	4	7500	100	75	188
CO	Silica	100-200	250	$Cu\text{-}ZnO/Al_2O_3$	2.5	4762[c]	98	-	[191]
CO	Silica	300	280	CuO/CeO_2	1	2000	95	-	187
CO	Silica	300	280	CuO/CeO_2	1	2070	95	<88	189
CO	Silica	0[d]	280	$Cu\text{-}ZnO/Al_2O_3$	1	8333[c]	~95	-	186
CH_4	Co-doped silica	500	500	Ni	3	-	~75	98	197
CH_4	HMDS silica	100	500	Ni/Al_2O_3	2.5	-	80	-	45
CH_3OH	Silica	150	300	$Cu\text{-}ZnO/Al_2O_3$	3	6000	~87	-	169
$CH_3C_6H_{11}$	DMDPS silica	300	300	Pt/Al_2O_3	-	-	80	99.9	198
$CH_3C_6H_{11}$	Silica	100	220	Pt/Al_2O_3	-	-	80	-	199
$CH_3C_6H_{11}$	Hybrid silica	100	250	Pt/Al_2O_3	-	6.45	86	99.8	200
$CH_3C_6H_{11}$	Hybrid silica	300	270	Pt/Al_2O_3	-	-	42	99	201
$CH_3C_6H_{11}$	Hybrid silica	300	230	Pt/Al_2O_3	-	4.53	55	-	177
C_6H_{12}	Hybrid silica	300	312	Pt/Al_2O_3	-	16.3	80	99.9	202
C_2H_5OH	$SiO_2\text{-}Al_2O_3$	101	350	Na–Co/ZnO	1.5	3.864[b]	60	99.8	105
C_2H_5OH	$SiO_2\text{-}Al_2O_3$	101	350	Na–Co/ZnO	6.5	6000	~85	~72	203

[a] *S/C* ratio, Steam to carbon ratio
[b] WHSV, weight hourly space velocity (h^{-1})
[c] GHSV, Gas hourly space velocity ($\times 10^3$ cm^3 h^{-1} $kg\text{-}cat^{-1}$)
[d] Sweep gas was used to generate H_2 pressure difference

Aside from methane and alcohols, H_2 can also be derived from other organic compounds. One that has been studied in detail is cyclohexane. TEOS-, TMOS- and DMDPS-derived silica membranes have been shown to successfully enhance cyclohexane conversion.[38, 177] Methylcyclohexane is also a promising feedstock as it has a high hydrogen density and can undergo reversible hydrogenation–dehydrogenation reactions.[200] Oda *et al.*[198] found that employing DMDPS-derived silica membranes to assist the dehydrogenation of methylcyclohexane could achieve the same level of conversion as traditional reactors but at slightly lower (20 °C lower) operating temperatures. Akamatsu *et al.*[201] demonstrated that DMDPS-derived silica membranes could maintain the same level of methylcyclohexane conversion (40%), H_2 purity (99%) and H_2 yield (5 cm^3 min^{-1}) over 1054 h. Li *et al.*[199] demonstrated that in the presence of a TEOS-derived silica membrane, it was possible to achieve full methylcyclohexane conversion at ~240 °C (60 °C lower than that required in a conventional reactor). The TEOS-derived membrane has also been widely used to promote methanol and ethanol reforming.[105, 169, 195, 203] Nomura *et al.*[39] observed an increase in HI conversion from 25% to 76.4% when decomposing HI in the presence of a TEOS-derived silica membrane at 600 °C.

Despite the success of lab work employing silica membranes to enhance H_2 production, one drawback that has to be resolved is its negative interaction with steam. At elevated temperatures, steam reacts with silica and transforms the siloxane groups (-Si-O-Si-) to silanol groups (Si-OH) which are more hydrophilic. The mobile silanol group may close off narrow pores and enlarge wide pores. This leads to poor hydrothermal stability and low selectivity of H_2.[204] In order to

prevent the motion of silanol groups in the silica matrix, great efforts have been devoted to incorporating metal or metal oxide into the silica. The nanoparticles of metal oxide in the silica matrix may reduce water sorption and resist the motion of Si-OH.[205] Co-doped silica[14, 29, 81, 85, 180, 181, 205-212], Ni-doped silica[184, 213] and Niobia-doped silica[214-216] which contain embedded Co, Ni and Nb oxide nanoparticles in the silica matrix, respectively, have been found to be effective at improving the hydrothermal stability of silica-derived membranes.

3.3 Other membrane reactors

Aside from palladium and silica, zeolite thin films are also a potential candidate for H_2 separation membranes (Fig. 8).[217] Zeolites are crystalline inorganic framework structures that have uniform molecular-sized pores. The size of the pore is categorised by the number of framework atoms in each aperture ring. Small-pore zeolites include structures made up of six-membered (~0.28 nm) or eight-membered rings (~0.42 nm), medium-pore zeolites have 10-membered rings (~0.57 nm), and large-pore zeolites have 12-membered rings (0.7~0.74 nm).[218, 219] Zeolite can efficiently sieve H_2 molecules from other gases with the appropriate pore size and orientation.

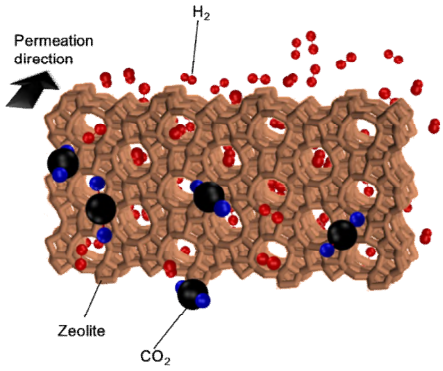

Fig. 8. Schematic of zeolite membrane separation mechanism.

Illgen *et al.*[220] investigated the performance of a Zeolite Socony Mobil with sequence number five (MFI) membrane (ZSM-5) for assisting the dehydrogenation of iso-butane. The selectivity of H_2 over iso-butane was reported to be 70 at 510 °C, and the conversion of iso-butane was doubled. Liu *et al.*[221] performed CO_2 reforming of methane in a zeolite membrane reactor and observed an enhancement in CH_4 conversion of ~20% above that of a standard fixed-bed reactor along with a separation factor between H_2 and CH_4 of 9.2. Jeong *et al.*[222] fabricated Faujasite (FAU)-type zeolite membrane to assist dehydrogenation of cyclohexane. The cyclohexane conversion was successfully promoted beyond the conventional thermodynamic equilibrium value by more than 30 % at 225 °C. However, despite the membrane blocking cyclohexane, it allowed benzene to permeate through, necessitating additional purification steps to separate the benzene from H_2. In order to improve the selectivity of H_2 over other gases with zeolite membranes, mono silica can be deposited onto the zeolitic channels to reduce their pore size.[223, 224] Tang *et al.*[225] used this method to reduce the pore sizes of an MFI zeolite membrane down to < 0.36 nm and witnessed an increase in H_2/CO_2 selectivity from 4 to over 60. Deployment of this membrane to enhance WGS increased the CO conversion to 81.7% from the 62.5% observed in a conventional packed-bed reactor. Kim *et al.*[226] used the same type of membrane but with a lower H_2/CO_2 selectivity (~10) to study the effects of operating conditions on the WGS reaction. Their results suggest that membranes with moderate H_2 selectivity can be effective for enhancing CO conversion at operating temperatures over 450 °C. Moreover, stable CO conversion in the presence of 1000 ppm H_2S was achieved during a 100-h test.

The most difficult step during the synthesis of zeolite membranes is the minimisation of intercrystalline pores between the grain boundaries.[227] The existence of intercrystalline pores with sizes much greater than the diameter of undesirable gases is the major culprit for the loss in separation efficiency. Currently, there is ongoing research into techniques to resolve this issue. These include epitaxial growth,[228] seeding with secondary growth,[229, 230] template-free secondary growth,[231] template/solvent removal[232] and post-synthesis repairing.[233]

Carbon-based membranes are another promising candidate for hydrogen separation since they have excellent thermal resistance, and separation performance.[234] Numerous synthetic precursors have been used to form carbon membranes. These include polyimide and derivatives,[235] polyacrylonitrile (PAN),[236] phenolic resin,[237] polyfurfuryl alcohol (PFA),[238] polyvinylidenechloride-acrylate terpolymer (PVDC-AC),[77] phenolformaldehyde,[239] and cellulose.[240] These precursors are heated under a controlled atmosphere and undergo pyrolysis to create a microporous structure. Carbon membranes tend to deteriorate severely if exposed to trace organics or strongly adsorbing vapours,[241] so they are preferentially used under non-oxidising environments.[44]

Zhang *et al.*[242] prepared a carbon-based membrane from a mixture of N,N-dimethyl formamide (DMF), phenol formaldehyde novolac resin (PFNR) and polyethylene glycol (PEG) to assist SMR and observed a H_2/CO selectivity of up to 108. Full conversion of methanol was achieved at only 250 °C, which represents a substantial reduction in energy requirement relative to conventional processes (T > 300 °C[243]). Sá *et al.*[244] produced a carbon membrane by pyrolysis of dense cellulose hollow fibres, followed by carbon chemical vapour deposition to achieve optimal pore sizes for improving H_2 selectivity. The membrane was used to enhance methanol steam reforming at 200 °C, reaching full conversion with low feed flow rates (30 cm^3 min^{-1}) and represents approximately a 100 °C reduction in operating temperature compared to that required for a conventional methanol steam reforming reactor. The CO concentration in the effluent was found to be less than 20 ppm, which suggests the H_2 selectivity was improved with their methodology. Hirota *et al.*[245] prepared a carbon membrane using furfuryl alcohol (FFA) as the carbon source and improved its H_2 permeability through post-synthesis activation under atmospheres of H_2, CO_2, O_2 and steam. The membrane thickness was reduced when it was activated in the CO_2 and O_2 atmospheres but not in H_2 and steam. However, activating the membrane with H_2 and steam increased the pore sizes of the FFA membranes from 0.3 to 0.45 nm which resulted in a better H_2 permeability. Methylcyclohexane dehydrogenation at 200 and 220 °C in the presence of the H_2-activated membrane gave methylcyclohexane conversions of 50% and 60%, respectively. This was a marked improvement over the 20% and 40% conversions observed at the same temperatures in the traditional reactor. D'Angelo *et al.*[246] conducted aqueous-phase reforming (APR) of sorbitol in a carbon-coated alumina membrane reactor derived from polymerised FFA. Over 2.5 times more H_2 was produced than from a traditional reactor under the same conditions (25×10^5 Pa, 220 °C). Furthermore, the hydrophobic nature of the membrane helped avoid water adsorption and minimised the interaction between the ceramic support and water, hence reducing the risks of membrane degradation.

4. Shift effect by CO_2 capture

One of the most widely investigated methods of removing CO_2 *in situ* from H_2-producing reactions is with solid sorbents.[21] One advantage of solid sorbents over membranes is that they are easier to uniformly distribute inside a reactor, thus giving a more uniform shift effect. As depicted in Fig. 9, removal of CO_2 shifts the reaction equilibrium towards the production of H_2 and further conversion of CH_4 and H_2O.

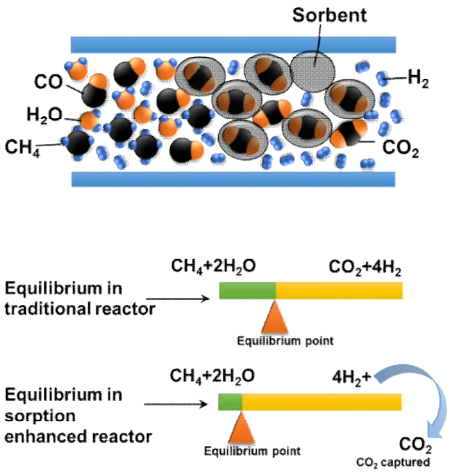

Fig. 9. Schematic of component equilibrium shift during SMR (Eqn. 3) by CO_2 capture.

However, unlike membranes, which require a small amount of material to allow the permeation of H_2, a much larger quantity of material may be required to capture CO_2 depending on its uptake capacity.[97] Consequently, low-cost, abundant sorbent materials which have high CO_2 carrying capacities are preferred.[247] In addition, the sorbent must be chemically and thermally stable to resist the high operating temperatures and reactive gases. In the case of a fixed-bed reactor, the use of sorbents can be less flexible in terms of continuous operation compared to utilising membranes. Once the sorbent has captured CO_2, the CO_2 must be desorbed in a parallel reactor to prevent CO_2 release contaminating the H_2 product gas. In a parallel system, once the sorbent in one reactor becomes saturated, the reactant gas flow can be switched into a second (or third) reactor while the sorbent in the first reactor is regenerated under an inert atmosphere. Provided the switchover is smooth, it is possible to achieve continuous production of H_2 (Fig. 10).

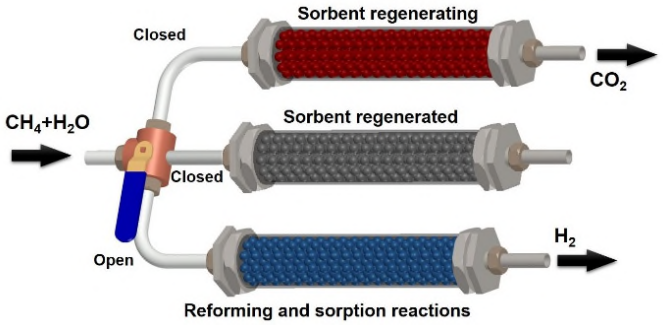

Fig. 10. Configuration of parallel fixed-bed reactors to enable continuous H_2 production.

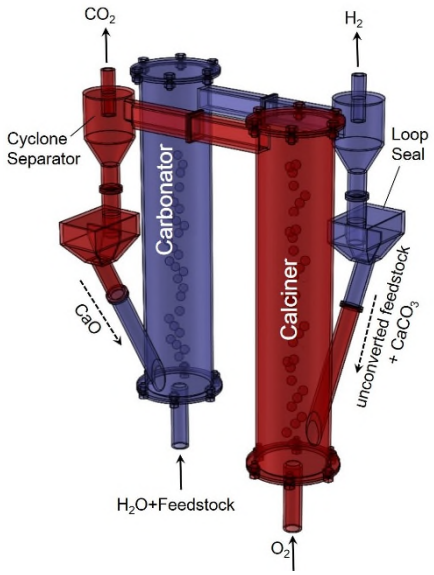

Fig. 11. Configuration of calcium looping with two circulating fluidised beds for H_2 production

An alternative method for continuous operation is through the use of two interconnected circulating fluidised beds to loop the solid between a gasifier/SMR/WGS/carbonator reactor and a regenerator/calciner. Using high velocities to transport the solids eliminates the difficulties associated with reactor switchover present in the fixed bed systems. One example of a high-temperature solid looping process is the calcium looping cycle (Fig. 11).[248] Calcium looping has been implemented in a number of studies to enhance the production of H_2 by continuously removing CO_2 during gasification,[249-253] and steam methane reforming.[254-256] In this system, gaseous or solid hydrocarbon feedstock is continuously fed into the carbonator/reformer reactor (~600-700 °C), which is loaded with CaO-based sorbents. The CaO reacts with the CO_2 (Eqn. 17) produced from either gasification or reforming/WGS to form $CaCO_3$ and H_2 gas (assuming complete reactions).

$$CaO + CO_2 \leftrightarrow CaCO_3 \quad \Delta H^0_{298} = -179 \text{ kJ mol}^{-1} \tag{17}$$

Hence, this yields an overall reaction equation in the reformer as:

$$\text{Hydrocarbon} + CaO + H_2O \rightarrow CaCO_3 + H_2 \tag{18}$$

The $CaCO_3$ is then passed through a cyclone and into the calciner (~850-950 °C) where it is decomposed back into CaO and CO_2, with the supply of heat (Eqn. 19).

$$CaCO_3 + O_2 \text{ and fuel or heat} \rightarrow CaO + CO_2 \tag{19}$$

This CO_2 is removed and can then be purified and compressed, ready for transportation and storage, while the regenerated CaO is circulated back into the carbonator where it participates in CO_2 capture again. The heat required in the calciner is typically supplied through oxy-fuel combustion of additional fuel.

One point of concern with this process is the high sorbent regeneration temperatures.[257] Under these conditions, the sorbent is prone to sintering, which results in pore closure and loss of activity/capture capacity. This can be exacerbated in an atmosphere of CO_2 and steam.[258] Consequently, it is essential to develop/employ materials which demonstrate good sintering resistance, especially when the goal is to achieve long-term stable operation. High sorption capacities are also favourable as they allow longer breakthrough times, reduce the quantity of sorbent, and reduce the frequency of switchovers/circulation rates between reactors. To achieve high H_2 productivity, high reactant flow rates are preferred, meaning that fast CO_2 sorption/desorption kinetics are essential.

4.1 Application of CaO-based sorbents

CaO has been considered one of the most promising candidates for sorption-enhanced steam methane reforming (SESMR) because of its low cost, availability, high theoretical CO_2 sorption capacity and fast sorption kinetics.[247] The reaction between CO_2 and CaO is given by Eqn. 17.

The sorption reaction typically occurs at 600-700 ^oC at atmospheric pressure, and the regeneration reaction takes place at 850-950 ^oC. The maximum theoretical CO_2 sorption capacity (mass of CO_2 per mass of sorbent) is 0.78 g/g CaO.[259] Despite these attractive characteristics, its practical application is confronted with various issues such as loss of sorption carrying capacity during long-term cyclical operation owing to sintering, attrition and potential competing sulphation reactions (if a high sulphur feedstock is utilised).[247] The sintering problem is primarily due to the low Tammann temperature of $CaCO_3$ (533 ^oC), which is the temperature above which sintering can thermodynamically occur.[247] This sintering effect causes its pores to collapse which leads to pore blockage, and a reduction in pore volume, pore connectivity and active surface area.[260] Furthermore, the CaO can never achieve 100% conversion since the molar volume of the product $CaCO_3$ is greater than CaO and the particles shrink during repeated reactions. Part of the product layer also grows into the pores and inhibits carbonation.[261, 262] In view of these drawbacks, great efforts have been devoted to incorporating inert spacers with very high Tammann temperatures to disperse CaO. So far, research has shown that supporting the active CaO on Al_2O_3,[263] MgO,[264] TiO_2,[265] SiO_2,[266] Y_2O_3,[267] La_2O_3,[268] $CaTiO_3$,[269] $Ca_9Al_6O_{18}$,[270] $Ca_3Al_2O_6$,[271] $Ca_{12}Al_{14}O_{33}$,[257] $CaZrO_3$,[272] Ca_2SiO_4,[259] $MgAl_2O_4$,[273, 274] $KMnO_4$[275] and aluminate cement[276] can improve its cyclic stability under certain conditions.[277]

Table 3 summarises the key results from studies which used CaO-based sorbent to enhance H_2 production from various thermochemical processes. Approximately two decades ago, Balasubramanian *et al.*[278] utilised high-purity $CaCO_3$-derived CaO sorbent and a Ni-Al_2O_3 catalyst for SESMR, achieving a maximum CH_4 conversion of 95%. This conversion gradually reduced to ~73% in the post-breakthrough period. The CaO conversion was reported to be only ~52% at the point of breakthrough. Particle agglomeration and pore closure caused by sintering and/or product layer formation were the likely culprits for failing to achieve higher CaO conversions. Owing to the low CaO conversion observed in the initial test, cyclical operation was abandoned in this study.

Dolomite and limestone which contain $MgCO_3$ and SiO_2 are also attractive options owing to their high thermal stability.[279, 280] The natural existence of inert spacers such as $MgCO_3$ or SiO_2 in dolomite and limestone was found to improve long-term cyclability of the CaO sorbents. He *et al.*[281] examined the performance of dolomite for enhancing ethanol steam reforming over 8 cycles (*S/C* = 3, carbonation at 575 ^oC, and calcination at 770 ^oC for 30 min in Ar). Although pure H_2 was produced in each cycle, the pre-breakthrough periods diminished with the cycle number. This was due to the deterioration of CO_2 capacity. The CO_2 capacity decreased by ~50% from the 1st cycle to the 8th cycle, but remained invariant in the last 3 cycles. Pimenidou *et al.*[282] used dolomite to enhance the reforming of waste cooking oil over six cycles. Their test showed consistent fuel conversion and H_2 purity, with a carbonation efficiency of ~56% in the last cycle. Lopez Ortiz *et al.*[283] employed dolomite in a fixed-bed reactor to enhance SMR over 33 cycles whereby the reactor had its temperature cycled between 800 ^oC for H_2 production/carbonation and 950 ^oC for sorbent regeneration under pure CO_2 conditions for 5 min each. The CaO conversion was maintained above 80% in the first 10 cycles and stayed above 50% after 25 cycles. Fermoso *et al.*[284] demonstrated that there was only a small reduction of pre-breakthrough time from 145 min to 135 min when they used dolomite to enhance crude glycerol reforming over three cycles.

Table 3. Operating conditions and performance of sorption-enhanced reactor with CaO-based sorbents.

Feedstock	Material	Pressure	Reaction conditions (°C)		Breakthrough	*S/C*	Feed rate	Conversion	H_2 purity	Cycles	Reference
		(kPa)	Sorp.	Desorp.	(min)		(cm^3 min^{-1})	(%)	(%)		
CH_4	CaO/Ni	1515	650	-	70	4	200	97	95	1	278
CH_4	Dolomite/Ni	1515	650	800	70	4	500	-	95	25	283
CH_4	CaO-$Ca_{12}Al_{14}O_{33}$/Ni	101	630	850	55-60	5	72	-	~95	12	285
CH_4	Dolomite/Ni	101	600	850	150	3	384[a]	-	98	4	286
CH_4	CaO-$Ca_{12}Al_{14}O_{33}$/Ni	101	650	850	110	3.4	158	>90	~92	13	287
CH_4	CaO-$Ca_{12}Al_{14}O_{33}$-Ni	101	650	850	~130	3.4	167	97	90	1	288
CH_4	CaO-Ni	101	600	-	10	3	50	90	80	1	289
CH_4	La_2O_3-CaO-Ni-Al_2O_3	101	600	800	-	4	257[a]	~80	~92	30	290
CH_4	ZrO_2-CaO-Ni-Al_2O_3	101	600	800	-	4	1800[a]	93.7	90	20	158
CH_4	CaO-Ni-HTlc	101	550	750	150	4	560	-	99	10	291
CH_4	CaO-Ni-$Ca_{12}Al_{14}O_{33}$	-	630	777	40	3	280	-	95	4	292
CH_4	CaO/Ni-HTlc	101	550	750	250	4	560	-	99	10	293
CH_4	CaO-$Ca_9Al_6O_{18}$/Ni-HTlc	101	550	800	45	4.2	76	~97	97	1	254
CH_4	CaO-$Ca_9Al_6O_{18}$/Ni-Al_2O_3	101	650	850	10	2.85	1617	-	89.1	1	294
CH_4	CaO-$Ca_9Al_6O_{18}$/Ni-MgAlO	101	600	800	60	4	78	~97	98	35	295
CH_4	CaO-$Ca_{12}Al_{14}O_{33}$/Ni-HTlc	-	550	750	110	4	560	-	99	10	296
CH_4	CaO-Ni-$Ca_9Al_6O_{18}$	100	650	800	50	4	175	100	95	30	297
CH_4	CaO-Ni-$CaZrO_3$	100	650	800	18	4	150	100	95	10	298
CH_4	CaO-$Ca_9Al_6O_{18}$/Ni-$Ca_5Al_6O_{14}$	100	650	800	20	3	1594[b]	94	93	60	299
CH_4	CaO-Ni	-	650	-	10	3		96.66	90	1	300
CH_4	CaO-Ni	101	650	-	~15	3		~95	~78	1	301
CH_4	CaO-Ni-$Ca_5Al_6O_{14}$	100	650	800	60	4	78	97.5	96	10	302

CH_4	CaO-Ni-$CaZrO_3$	100	600	800	~60	3	66	90	95	10	303
CH_4	CaO-Ni-$CaZrO_3$	101	600	850	30	3	24	~82	90	5	304
CH_4	CaO-Ni-MMT	101	650	700	50	3	150	100	85	1	305
CH_4	CaO-$CaZrO_3$/Ni-ZrO_2	101	650	800	50	3	250	98	95	20	306
Coal	CaO-MgO-3A	101	650	900	-	-	0.3[d]	-	85	1	43
Glycerol	CaO- $Ca_{12}Al_{14}O_{33}$-Co	101	650	-	14	4	2.4[c]	86.5	96	50	307
Glycerol	Dolomite/Co-Ni	101	575	770	200	3	0.5	100	99	1	308
Glycerol	Dolomite/Ni	101	500	-	5	3	0.97	100	97	1	309
Glycerol	CaO-HTlc-Co-Cu	101	525	700	8	4	0.08	97.31	99.2	10	15
Glycerol	La_2O_3-CaO-Ni-Al_2O_3	-	600	900	-	-	-	-	70	5	310
Glycerol	Dolomite/Co-Ni	101	550	770	120	3	-	-	99.7	3	284
Glycerol	Limestone/Ni	101	550	900	10	3	-	-	99.8	6	311
Glycerol	Lime/Ni	101	600	-	10	3	0.064[c]	-	96.1	1	312
Bio-oil	CaO/Ce-Ni-Co-Al_2O_3	-	750	-	-	12	0.15[a]	-	90	1	63
Bio-oil	CaO/Pd/Ni–Co	101	575	-	-	3	0.893[c]	-	99.8	1	313
$C_2H_4O_2$/C_3H_6O	CaO/Pd/Ni–Co	101	575	900	-	1~10	0.4-2.8	-	99.2	1	314
C_2H_5OH	CaO-Al_2O_3/Co	101	550	-	-	3	500	-	>75	1	61
C_2H_5OH	CaO-Ni-Al_2O_3	101	600	-	125	3	414	-	96.6	1	315

[a] (h^{-1})

[b] Unit is $cm^3\ g^{-1}\ h^{-1}$

[c] WHSV, weight hourly space velocity (h^{-1})

[d] Liquid phase flow rate

As noted above, synthetic sorbents formed from the combination of CaO and an inert stabiliser have been identified as the most popular route towards improving the sorbent thermal stability. A CaO-$Ca_{12}Al_{14}O_{33}$ sorbent synthesised by Martavaltzi *et al.*[287] *via* an impregnation method was mixed with Ni catalyst and tested for SESMR over 15 cycles (at 1×10^5 Pa, *S/C* = 3.4, 650 °C). After an initial dip, the CO_2 capacity was found to stabilise at around 37 wt.% after the first 5 cycles. The pre-breakthrough time in the last cycle was found to be 20% shorter than that for the 1st cycle. Wu *et al.*[158] prepared a ZrO_2-modified complex, ZrO_2-Ni-CaO by an impregnation method. This material demonstrated high-purity (>80%) H_2 production over 20 cycles with only around 10% deactivation (1×10^5 Pa, *S/C* = 4, 600 °C). The reference sorbent (an unmodified Ni-CaO sorbent without ZrO_2), experienced rapid deactivation after just three cycles.

In these sorption-enhanced reactions, it is necessary to mix the catalysts and sorbents in the reactor; however, achieving homogeneity to avoid chemical inter-diffusion and loss of activity during operation is extremely challenging.[142, 316] A solution to this is to combine the catalyst and sorbent into bifunctional catalyst-sorbent materials (or hybrid functional materials/composites). Combining the sorbent and catalyst together can shorten the distance between the catalytic site and the sorption site, thus reducing the time it takes for CO_2 to travel between them. These materials also allow immediate heat delivery from the exothermic capture site to the endothermic reforming site, giving a more uniform reaction profile. Dewoolkar *et al.*[317] compared the performance of a hybrid Ni/CaO sorbent with a powdered mixture of catalyst and sorbent in a tubular fixed-bed reactor. The hybrid functional material exhibited a longer breakthrough time (35 min *vs.* 10 min), higher CH_4 conversion and H_2 yield compared to powdered materials under identical conditions (1×10^5 Pa, *S/C* = 9, 500 °C). The cyclic stability of the hybrid material was found to benefit from the well-dispersed spacer. The performance of the mixture was found to match the performance of the hybrid functional material for the first 2 cycles, but its performance deteriorated rapidly owing to sintering effects. Radfarnia *et al.*[297, 298] examined the performance of the hybrid materials, CaO-Ni-$Ca_9Al_6O_{18}$ and CaO-Ni-$CaZrO_3$ for 30 and 10 cycles, respectively. The catalytic sorbents were found to give consistent H_2 purity over 90%, full CH_4 conversion and constant CO_2 capacity over all cycles.

4.2 Application of other sorbents

Aside from CaO-based sorbents, sorbents derived from alkali metal-based oxides, magnesium-based double salts and hydrotalcite have also been studied for enhanced H_2 production.[316] Most of this work has focused on the improvement of sorbent capacity, kinetics and stability. Although hydrotalcite sorbents were deemed to be unsuitable for SESMR owing to incompatible operating temperatures,[318] they have found a more useful role in enhancing WGS instead. van Selow *et al.*[319, 320] demonstrated that K_2CO_3-promoted hydrotalcites can achieve full CO conversion and pure H_2 production at 400 °C under 28×10^5 Pa and S/C = 1.6. The major issue with hydrotalcite-based sorbents is their low CO_2 capacities.[321] Mg-Al-CO_3 layered double hydroxides (LDH)-type sorbents, developed by Yong *et al.*[322] only captured ~0.022 g-CO_2/g-sorbent. Reddy *et al.* [323, 324] made further efforts to improve the CO_2 uptakes to 0.027 and 0.048 g-CO_2/g-sorbent for dry and wet conditions (15 vol.% CO_2), respectively. Additional improvements were achieved by adding promoters such as potassium, resulting in CO_2 capacities of ~0.051 g-CO_2/g-sorbent (12 vol.% CO_2 at 400 °C).[320] Although significant improvements were attained, these CO_2 capacity values are still too low compared with Ca-based sorbents.[325]

Alkali metals such as lithium- and sodium- based sorbents have also been intensively investigated as high-temperature CO_2 acceptors.[316, 326-331]

$$Li_4SiO_4 + CO_2 \leftrightarrow Li_2SiO_3 + Li_2CO_3 \quad \Delta H^0_{298} = -142 \text{ kJ mol}^{-1} \tag{20}$$

$$Li_2ZrO_3 + CO_2 \leftrightarrow Li_2CO_3 + ZrO_2 \quad \Delta H^0_{298} = -160 \text{ kJ mol}^{-1} \tag{21}$$

$$Na_2ZrO_3 + CO_2 \leftrightarrow Na_2CO_3 + ZrO_2 \quad \Delta H^0_{298} = -149 \text{ kJ mol}^{-1} \tag{22}$$

Li_4SiO_4, which has a relatively high CO_2 carrying capacity (0.367 g-CO_2/g-sorbent) compared to Na-based ceramic sorbents, was tested for SESMR by Essaki *et al.*[332] However, no clear shift effect was observed and the final CH_4 conversion after 30 min remained below the equilibrium value for conventional SMR at 600 °C (*S/C* = 3.5). Although Li_4SiO_4 has a high CO_2 capacity, its performance appeared to be hampered by its slow sorption kinetics.[236, 317, 318]

Na_2ZrO_3 has been regarded as a kinetically fast and stable CO_2 acceptor with a decent CO_2 capacity (0.238 g-CO_2/g-sorbent).[316, 326, 327, 333-335] Furthermore, it has been known to exhibit some catalytic ability for CO oxidation as well as methane reforming.[336, 337] Aceves Olivas *et al.*[315] demonstrated a maximum of 92.2% purity H_2 *via* steam ethanol reforming at 1×10^5 Pa, with a *S/C* ratio of 3 at 600 °C in a fixed-bed reactor using a combination of this sorbent and Ni/Al_2O_3 catalyst. This was marginally lower than the 96.6% and 94.4% H_2 purities obtained with CaO and CaO+MgO sorbents, respectively.

Application of Na_2ZrO_3 and Li_2ZrO_3 sorbents for SESMR was also studied by Ochoa-Fernández *et al.*[338] Over 95% H_2 purity was obtained using Na_2ZrO_3 sorbent at 5×10^5 Pa with *S/C* = 5 at 575 °C. On the other hand, no enhancement in the H_2 yield was observed in the presence of Li_2ZrO_3 due to its low CO_2 capture kinetics under low CO_2 partial pressure

environments. It was reported that interaction between the Ni catalyst and Na_2ZrO_3 resulted in catalyst deactivation, possibly due to the migration of Na ions and the consequent coverage on Ni-sites.

4.3 Bed utilisation of reactor

Initially, fresh sorbents have a high CO_2 sorption potential and are not kinetically limited; this defines the pre-breakthrough period shown in Fig. 12. Over time the sorption kinetics slow down with increased conversion owing to a loss in reactive surface area. In a fixed-bed system, where the sorbent is not continuously replenished, this reduced CO_2 sorption eventually leads to a reduction in H_2 purity and yield, defined as the breakthrough period. Once the sorbent saturates (and the shift effect terminates), the reactor performance returns to that of a traditional steam gasification/reforming reactor, shown as the sorbent saturation phase in Fig. 12.

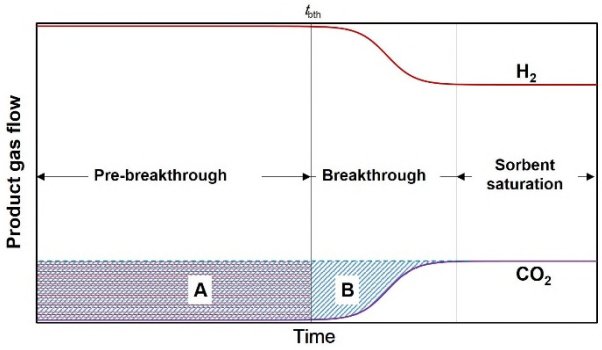

Fig. 12. Representative evolution of product gas from fixed-bed sorption reactor.

In order to maximise the purity of H_2 and to facilitate continuous operation of these sorbents, the reactor must switch over to the regeneration conditions before the breakthrough period begins. In doing so, part of the sorbent capacity is left unutilised. The bed utilisation factor (Eqn. 25) is used to quantify the percentage of the effective sorbent capacity and is a ratio of the CO_2 captured before the breakthrough occurs (area A) relative to the total CO_2 captured after saturation (area A and B).[325]

$$A = \int_0^{t_{bth}} \left(\frac{F_{CO_2,\infty} - F_{CO_2,t}}{F_{CO_2,\infty}} \right) dt \tag{23}$$

$$A + B = \int_0^{\infty} \left(\frac{F_{CO_2,\infty} - F_{CO_2,t}}{F_{CO_2,\infty}} \right) dt \tag{24}$$

$$X_{utl} = \frac{\int_0^{t_{bth}} \left(\frac{F_{CO_2,\infty} - F_{CO_2,t}}{F_{CO_2,\infty}} \right) dt}{\int_0^{\infty} \left(\frac{F_{CO_2,\infty} - F_{CO_2,t}}{F_{CO_2,\infty}} \right) dt} \tag{25}$$

Here, the bed utilisation factor is denoted X_{utl}, t_{bth} is the time when breakthrough begins and F is molar flowrate. The area B denotes the unutilised portion of CO_2 capacity. The duration of breakthrough is shorter for fast-kinetic CO_2 sorbent. It is clear from its definition that in order to maximise the useful bed capacity, not only are high CO_2 carrying capacities required but so are rapid sorption kinetics. This implies that materials with high CO_2 capacity but slow kinetics, such as Li_2ZrO_3 or Li_4SiO_4, are not suitable to enhance H_2 production.[247, 339, 340]

5. Synergistic enhancement by membrane permeation and CO_2 capture

In some recent studies, H_2 membranes and CO_2 sorbents were combined in the same reactor to enhance feedstock conversion and H_2 production.[341] This configuration has been defined as a sorption-enhanced membrane reactor (SEMR), hybrid adsorbent-membrane reactor (HAMR) or membrane-assisted sorption-enhanced reactor (MASER). With these hybrid setups, the driving forces are further increased. The inclusion of CO_2 sorbents in the membrane reactor may also introduce additional synergistic effects which could improve the overall reactor performance. For example, adding CO_2 sorbents into the membrane reactor will help shift CO into CO_2 *via* enhanced WGS. This is good for the membrane

material since CO can inhibit H_2 permeation in Pd membranes by disrupting the H_2 dissociation path,[91, 95, 103, 104, 173, 342-345] as well as lead to carbon deposition at low temperatures *via* the Boudouard reaction (Eqn 26).[65, 346] Carbon deposition can block gas flow and membrane permeation as well as deactivate catalysts.[325]

$$2CO \leftrightarrow C+CO_2 \quad \Delta H_{298}^{0} = -172.5 \text{ kJ mol}^{-1} \tag{26}$$

Incorporating sorbents into the same reactor may also relieve the effects of concentration polarisation in membrane reactors. Concentration polarisation, which results from the accumulation of nonpermeated gases at the interface of the membrane, is a common phenomenon in all membrane processes which reduces the membrane separation efficiency.[347] The build-up of nonpermeated CO_2 in the vicinity of the membrane can reduce the H_2 driving force across the membrane.[110, 345, 348] CO_2 sorbents can alleviate this problem by removing the CO_2 around the membrane.

The concept of hybrid enhancement by both membrane permeation and CO_2 sorption was initially explored using simulation studies. Chen *et al.*[349] developed a thermodynamic equilibrium model and a kinetic reactor model in Aspen plus™ to simulate *in situ*/*ex situ* removal of H_2 and/or CO_2 by a palladium membrane reactor with CaO sorbent. It was found that H_2 removal had a more significant effect in shifting the thermodynamic limit compared to CO_2 removal, given that equal moles of H_2 and CO_2 are removed. This is consistent with the expression given (Eqn. 6) in which the exponent of H_2 partial pressure is 4 times that of CO_2. The level of CH_4 conversion was found to follow the order of: sorption-enhanced membrane reactor > membrane reactor > sorption-enhanced reactor > conventional reactor. Prasad *et al*.[163] also simulated these four reactor configurations in fluidised beds and reported a similar order in CH_4 conversion performance, but with the standalone membrane and standalone sorbent setups the other way round. However, this comparison was not based on equimolar removal of H_2 and CO_2. Furthermore, a lower membrane area was assumed in the latter case (membrane area/reactor volume ratio: 10 m^2 m^{-3} for Prasad *et al*.[163] and 200 m^2 m^{-3} for Chen *et al*.[349]). Chen *et al.*[350] ran a 1-D simulation of SMR in a sorption-enhanced fluidised bed membrane reactor using the COMSOL solver to investigate the effects of operating pressure, total gas feed rate, solid recycle rate, fresh sorbent feed rate, effective membrane area and permeate pressure on the performance of a sorption-enhanced fluidised bed membrane. The model predicted that CH_4 conversions over 91% can be achieved for operating conditions of 6×10^5 Pa and 550 °C with low quantities of CO_2 and CO in the product. The sensitivity analysis of this model demonstrated that the membrane-assisted sorption-enhanced SMR is more heavily influenced by the membrane effectiveness rather the rate of CO_2 sorption.

Andrés *et al.*[351] for the first time, attempted the experimental demonstration of a fluidised-bed reactor with *in situ* removal of H_2 and CO_2 with palladium membranes and CaO for natural gas steam reforming. High-purity H_2 was not only obtained from the permeate side, but over 90 vol.% H_2 is was collected from reactor off-gas (retentate gas) ahead of the CO_2 breakthrough. This represents an obvious advantage over a standalone membrane reactor. This study also investigated the influence of limestone loading, membrane area and natural gas feed rates. The CH_4 conversion was increased under higher sorbent loading, and further enhanced when the membrane area was increased. The large size of the fluidised reactor they used limited the shift effect from membrane permeation owing to a low membrane area-to-reactor volume ratio. A compact design by combining catalyst and sorbents inside a membrane reactor which has a higher membrane area-to-reactor volume ratio was designed by García-García *et al.*[352] They deployed a Cu-based catalyst and hydrotalcite sorbent in a palladium membrane reactor to enhance WGS, observing >90% CO conversion for the sorption-enhanced membrane reactor. This was an improvement relative to the 80% conversion obtained in the sorption-enhanced reactor and the 50% conversion for a traditional fixed-bed reactor. However, undesired carbon formation was promoted, particularly with the reactors exhibiting higher conversions. This was ascribed to the low steam-to-carbon ratio (*S/C* = 0.75) used in their study. The excess CO tends to form C and CO_2 *via* the Boudouard reaction. Another possible reason might be that the hydrotalcite-derived Mg–Al mixed oxide sorbent adsorbed some of the H_2O and, therefore, reduced the *S/C* ratio indirectly. A similar study was undertaken by Soria *et al.*[353] but they reported less obvious effects of H_2O vapour on K_2CO_3-promoted hydrotalcite in a WGS environment. This work also compared the reaction performance between a sorption-enhanced WGS reactor and sorption-enhanced membrane WGS reactor under identical operating conditions at 3×10^5 Pa with *S/C* = 1.5 at 300 °C. The sorption-enhanced membrane reactor was found to outperform the standalone sorption-enhanced reactor. Moreover, the conversion was kept above the conventional equilibrium value even after the sorbents reached saturation because of the membrane.

6. Simulation of H_2 production from thermochemical processes

Generally, only measurements at the inlet and outlet of the reactor can be obtained experimentally. It is technically difficult to gain an insight of the reaction behaviour and the development inside the reactor. The internal behaviour is affected by operating conditions, reaction kinetics (Eqns. 5-7), H_2 permeation, CO_2 sorption, gas flow, as well as the reactor configuration. Consequently, it is necessary to take a modelling approach such as using computational fluid

dynamics (CFD) to predict the change in internal behaviour by solving a system of conservation equations which describe changes in fluid dynamics variables evolving with space and time. These include mass conservation, momentum conservation and energy conservation equations (Eqns. 27-30).

$$\frac{\partial c}{\partial t}+\frac{1}{r}\frac{\partial}{\partial r}\left(r\cdot c\cdot u_{\mathrm{r}}\right)+\frac{\partial}{\partial z}\left(c\cdot u_{z}\right)=S_{\mathrm{M}} \tag{27}$$

The mass conservation equation (Eqn. 27) relates gas concentration (c), and gas velocities in axial and radial directions (u_z, u_r) to the reaction source term (S_M), time (t) and space coordinate (z, r) by the principle of mass conservation.

$$\begin{aligned}&\frac{\partial u_{\mathrm{r}}}{\partial t}+u_{r}\frac{\partial}{\partial r}\left(\rho\cdot u_{\mathrm{r}}\right)+u_{\mathrm{z}}\frac{\partial}{\partial z}\left(\rho\cdot u_{\mathrm{r}}\right)\\&=-\frac{\partial p}{\partial r}+\eta\left[\frac{1}{r}\frac{\partial}{\partial r}\left(r\frac{\partial u_{\mathrm{r}}}{\partial r}\right)+\frac{\partial^{2}u_{\mathrm{r}}}{\partial z^{2}}-\frac{u_{\mathrm{r}}}{r^{2}}\right]+S_{\mathrm{r}}\end{aligned} \tag{28}$$

$$\begin{aligned}&\frac{\partial u_{\mathrm{z}}}{\partial t}+u_{\mathrm{r}}\frac{\partial}{\partial r}\left(\rho\cdot u_{\mathrm{z}}\right)+u_{\mathrm{z}}\frac{\partial}{\partial z}\left(\rho\cdot u_{\mathrm{z}}\right)\\&=-\frac{\partial p}{\partial z}+\eta\left[\frac{1}{r}\frac{\partial}{\partial r}\left(r\frac{\partial u_{\mathrm{z}}}{\partial r}\right)+\frac{\partial^{2}u_{\mathrm{z}}}{\partial z^{2}}\right]+S_{\mathrm{z}}\end{aligned} \tag{29}$$

The momentum conservation equations (Eqns. 28-29), which were known as the Navier-Stokes equations, connect pressure (p), and gas velocities (u_z, u_r) to the momentum source terms (S_z, S_r), gas viscosity (η), time (t) and space coordinate (z, r) by Newton's laws of motion.

$$\begin{aligned}&\frac{\partial T}{\partial t}+\frac{1}{r}\frac{\partial}{\partial r}\left(r\cdot T\cdot u_{\mathrm{r}}\right)+\frac{\partial}{\partial z}\left(T\cdot u_{\mathrm{z}}\right)\\&=\frac{k_{\mathrm{h}}}{\rho C_{\mathrm{p}}}\left[\frac{1}{r}\frac{\partial}{\partial r}\left(r\frac{\partial T}{\partial r}\right)+\frac{\partial^{2}T}{\partial z^{2}}\right]+S_{\mathrm{H}}\end{aligned} \tag{30}$$

The energy conservation equation (Eqn. 30) links temperature (T) with reaction heat source (S_H), heat conductivity (k_h), time (t), and space coordinate (z, r) by the law of energy conservation.

With appropriate boundary conditions, obtaining fluid dynamics information such as gas concentration, velocities, pressure and temperature at any time and location becomes possible by solving the equation set numerically. Thereby, using the distributed parameters rather than averaged or lumped values allows for a deeper understanding of the reaction process.

Another motivation for modelling the reactor processes is to aid reactor design. For instance, a common configuration in current sorption-enhanced reactors or sorption-enhanced membrane reactors uses uniform distribution of catalyst and CO_2 sorbent. However, this may not be optimal. García-García *et al.*[352] pointed out that using CO_2 sorbent in the first half of the reactor where the CO_2 partial pressure is low can be unnecessary. CO_2 sorption and H_2 permeation are only required when considerable CO_2 and H_2 have been produced and the initial reaction driving force reduces; however, at the inlet of the reactor, the gases have yet to react/come into contact with the catalyst. Consequently, it is more important to place more catalyst at the entrance to facilitate early reaction. CFD simulations can be used to model the partial pressure variations along the reactor and, therefore, optimise the catalyst-sorbent distribution scheme.

As mentioned earlier, concentration polarisation is a retarding effect resulting from the accumulation of less-permeable species and the depletion of the more-permeable species at the boundary layer near the membrane surface. It reduces the separation efficiency and is dependent upon the performance of the membrane as well as the operating conditions.[86, 110, 354] Since measuring the gas concentration distribution is difficult, a number of studies have adopted CFD simulation to investigate its effect on H_2 separation using Pd membranes.[93, 173, 355] Serious concentration polarisation effects were reported in each study. Moreover, the simulations suggest that it can be potentially exacerbated in the presence of a packed bed of catalyst since the mass transfer of gases from the bulk to the membrane is retarded.[345, 356]

Koukou *et al.*[357, 358] developed a two-dimensional (considering both axial and radial variation) cylindrical CFD model which incorporated the effect of concentration polarisation in a WGS reactor, and a simplified model assuming plug flow without concentration polarisation as a reference. It was found that the two-dimensional model predicts reduced H_2

transport rates through the membrane. Radial profiles of H_2 partial pressure were found to be very steep close to the membrane reactor inlet. This suggests that the product conversion and hydrogen recovery predicted by the two-dimensional model were found to be much lower than the respective values calculated by the simplified plug flow model. This study highlighted the importance of accounting for concentration polarisation during membrane reactor design. Following this, a number of CFD simulations have been devoted to addressing this issue in H_2 separation processes.[93, 96, 354, 359] The modelled flow field in the Coroneo *et al.*[355] simulation suggested that the installation of baffles may increase the turbulence and suppress the development of a concentration boundary layer, thereby relieving concentration polarisation and improving hydrogen permeation. However, in a packed-bed membrane reactor, the turbulence created by the baffle may vanish due to the resistance imposed by the packed particles. There has not yet been any effective approach to minimise concentration polarisation in packed-bed membrane reactors. Besides the concentration boundary layer, the temperature distribution in a membrane reactor is also of key importance. Koukou *et al.*[360] examined the temperature profile for cyclohexane dehydrogenation in a packed-bed membrane reactor. The radial profile of temperature was found to be similar to the concentration profile, showing a downward trend towards the membrane surface. This is due to the fact that the dehydrogenation reaction is endothermic and is more prominent in the direct vicinity of the membrane. The simplified plug-flow model, which did not consider radial variation, was found to overestimate the temperature field and feedstock conversion, necessitating the use of CFD simulations to analyse the performance of membrane reactors. A detailed simulation of WGS in a Pd membrane reactor was undertaken in COMSOL by Chen *et al.*[361] The output of the CFD model was successfully validated against available experimental data for the temperature profile along the membrane under the same operating conditions as 1×10^6 Pa, S/C = 3, $T_{r,in}$ = 500 °C, $T_{p,in}$ = 150 °C. This simulation was aimed at demonstrating the distribution in temperature, reaction rate and reaction driving force from $T_{r,in}$ = 400-600 °C when S/C = 2. The distributions of the H_2 and CO fractions in the reactor were also systematically analysed to elucidate how these results change with reactor inlet temperature (400-600 °C). Their work predicted that the WGS reaction proceeds from a kinetically-controlled process to thermodynamically-governed process when the feed gas temperature increases.

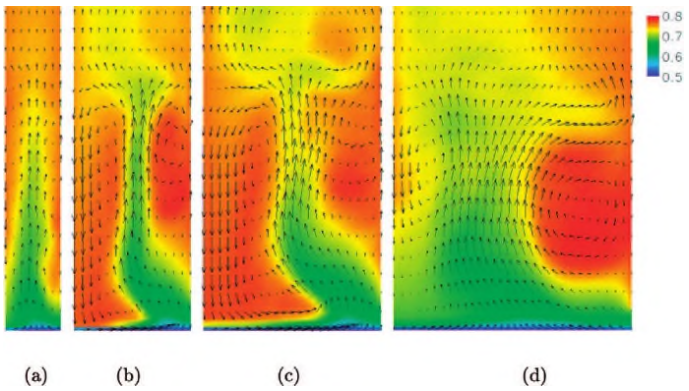

Fig. 13. Hydrogen mole fraction and gas velocity field in reactors of the following inner diameters: (a) 0.23, (b) 0.47, (c) 0.70, and (d) 0.92 m. The centre of the reactor is located to the left. Reproduced from Lindborg *et al.*[362]

As discussed above, fluidised-bed reactors were used to overcome the limitation of heat and mass transfer in packed beds, so a number of multiphase (gas and solids) CFD simulation studies were performed to analyse the process in fluidised-bed reactors as well. Xie *et al.*[363] simulated coal gasification by air and steam in a 2 m high fluidised-bed reactor. The particle flow patterns, profile of particle species, distributions of gas composition, heterogeneous and homogeneous chemical reaction rates and carbon consumption were predicted to give an insight into the complex process. Di Carlo *et al.*[364] built a CFD model to simulate SESMR with fluidised Ni catalyst and dolomite particles. The flow disturbance, gas concentrations, temperature and CH_4 conversion were examined in this study assuming a constant total solid inventory and variable dolomite/Ni ratio. This work found that increasing the sorbent ratio may raise the temperature and drop the CO_2 fraction, thereby improving CH_4 conversion and the outlet fraction of H_2. However, too high a ratio of dolomite decreased the Ni catalyst concentration and leads to poorer catalytic performance. $m_{Dolomite}/m_{Ni}$ = 2 was found to be the optimum ratio for obtaining both a high CH_4 conversion and H_2 purity. Lithium zirconate was adopted in the fluidised bed simulation of Lindborg *et al.*[362] It was found that variations in bed diameter had a minor influence on the outlet hydrogen concentration. Since wider reactors could process more gas, increasing the diameter is the most favourable choice for industrial applications. As is known, high pressure favours sorption kinetics but hinders conversion equilibrium.[67, 76] The simulation suggested that elevated operating pressures lead to a deteriorated performance in terms of H_2 purity. A key contribution of this simulation is the detection of flow patterns in the reactor, which exhibit gas recirculation (Fig. 13). Recirculation may reduce the reaction driving force as it mixes the product gas with reactant gas. However, if the recirculation zone is located away from the inlet, it can potentially extend the residence time. The observed recirculation

in the vector map of Fig. 13 also points out the inadequacy of using simplified 1-D models to simulate fluidised bed reactors, and demonstrates the importance of 3-D simulations. Wang *et al.*[365] performed a 3-D fluidised bed simulation for sorption-enhanced SMR. The simulation results revealed a heterogeneous bed structure and presented non-axial symmetric solid flow. This further confirms that more 3-D simulations are required to achieve a better understanding of flow in fluidised bed reactors.

7. Challenges and improvement directions

Although the improvement in H_2 production through H_2 and/or CO_2 removal has been largely successful, most tests have only been performed at laboratory scale. There are only a limited number of pilot-scale demonstrations.[251, 366-371] One example is the EU-funded STEPWISE H2020 project, which utilises sorption enhanced water gas shift (SEWGS) technology.[372] The STEPWISE project aims to remove 14 t d^{-1} CO_2 and produce a hot, pressurised H_2-rich stream suitable for power production. Demonstrating the feasibility of this process will help reduce speculation over risks associated with commercialisation. The main issues that need to be addressed to scale up these novel H_2 production technologies include cyclical stability, chemical/heat resistance, mass transfer limitations, possible interactions between sorbent and catalyst, imperfections in membrane layers, carbon deposition and overall process integration/optimisation. To close the gap between experimental investigation and large-scale implementation, further research should be devoted towards material development, process optimisation and engineering requirements.

7.1 Material synthesis

A number of synthesis techniques such as impregnation[290, 301, 373] and co-precipitation[31, 311] have been adopted to enhance the material stability, maximise the function of each component and improve the uniformity of catalyst, sorbent and stabiliser. However, the material uniformity (or dispersity) in these techniques is limited by the presence of solids, since the fluid-solid interaction depends on the solid particle size. Dissolving the precursors into clear solution would allow more homogeneous mixing and thorough reactions between precursors.[259, 327, 374] Consequently, solution-based synthesis routes could be an option for manufacturing next-generation hybrid-functional material. In addition, advanced drying techniques such as spray drying, freeze drying and supercritical drying which favour porous structure development, resulting in high surface area and pore volume, would facilitate mass transfer and expose more catalytic sites and sorption sites for the thermochemical conversion reactions.[375]

7.2 Process simulation

The design of reactors and determining optimal operating conditions are of great importance in developing an efficient H_2 production process. Understanding the influence of the main operating parameters through computer simulations will increase the certainty in the design and construction of unit operations for scaling up. Of course, these studies should be combined with experimental measurements to validate the simulation outcomes.

Relative to large-scale experimental demonstrations, simulations offer an inexpensive and less physically-intensive route towards the same goal. One example where simulation work could save time is validating a hypothesis mentioned by García-García *et al.*[352] They suggested that uniform distribution of catalyst and sorbent along a fixed-bed reactor will not be the optimal configuration. Most of the gasification/reforming/WGS reactions occurs towards the feedstock inlet of the reactor, so it is more logical to have catalysts positioned near the reactor inlet and sorbents/membranes further down the reactor. By simulating the reactor configuration and predicting the H_2 yield the extensive lab work associated with manually readjusting the reactor content could be avoided.

Each membrane material examined so far has shown weaknesses: Pd is susceptible to CO and H_2S poisoning, silica has low H_2 permeability, and zeolite and carbon membranes exhibit low selectivity towards H_2. Placing membranes in series may show synergistic effects and potentially offset certain weaknesses. For example, having a silica membrane in the first half of the reactor and a Pd membrane in the second half may potentially minimise exposure of the Pd membrane to CO since the CO concentration decreases along the reactor as it reacts. Running CFD simulations for this type of multi-membrane system would gain valuable insight before experimental implementation.

7.3 Engineering perspective

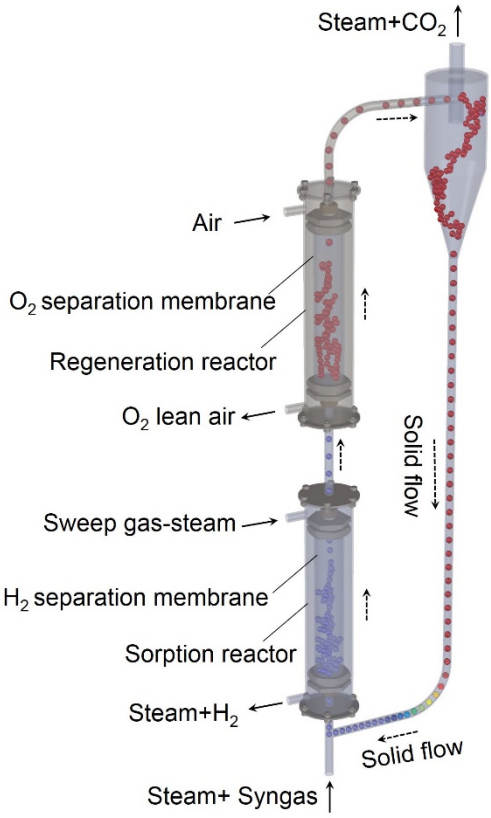

Fig. 14. Proposed reactor configuration for continuous H_2 and CO_2 production.

Since the hybrid membrane-sorbent reactor has been proved to be more effective in enhancing H_2 yield than standalone membrane reactors or sorption-enhanced reactors, developing the hybrid membrane-sorbent reactor will be worth investigating for H_2 production. However, most research on hybrid membrane-sorbent reactors has been conducted using fixed-bed reactors. This configuration suffers from process discontinuity, risk of flow blockage, and reduction of catalyst effectiveness and sorption capacity.[163, 164, 325] Fluidised-bed reactors do not have some of these problems, but the CO_2 sorbent will still saturate and must be replenished. Developing a circulating fluidised-bed system with two reactors in series enables continuous sorbent regeneration and CO_2 capture (Fig. 14). The first reactor (bottom) functions as the sorption-enhanced membrane reactor. It combines a H_2-selective membrane with fluidised catalyst-sorbent particles to produce pure H_2. The reactor off-gas and spent solid are then fed to a high-temperature second reactor (top) for sorbent regeneration. Since the H_2 recovery in the first reactor is less than 100%, the unrecovered H_2 portion can be combusted in the second reactor to provide energy for regeneration. If air is fed to combust this portion of H_2, N_2 as unwanted impurity is introduced to this system; however, if pure O_2 is fed to the second reactor, high-purity CO_2 can be produced (after the steam is knocked out). Installing an oxygen separation membrane such as fluorite-based or perovskite-based ceramic membranes[376] would allow this system to produce pure H_2 and pure CO_2 simultaneously. So far most fluidised-bed membrane experiments have utilised a single reactor.[131, 142, 209, 351] This research can be used as a starting point for developing dual circulating fluidised-bed membrane reactors to continuously generate pure H_2 and CO_2.

8. Conclusions and perspectives

H_2-selective membranes and CO_2 solid sorbents have been extensively investigated not only for the purpose of H_2 purification and CO_2 capture, but also for improving the single-pass H_2 yield. However, H_2 production is typically achieved *via* thermochemical reversible reactions such as SMR and WGS and is, therefore, limited by thermodynamic equilibria. According to Le Chatelier's principle, removing the products *in situ* overcomes the equilibria limitations and leads to higher feedstock conversions and enhanced H_2 production.

The utilisation of H_2-selective membranes in a hydrogen production vessel allows continuous withdrawal of H_2 and also results in high-purity H_2 production. This review critically assessed the performance of membrane reactors made from four types of materials: Palladium, Silica, Zeolite and Carbon. Each of these membranes have demonstrated improved feedstock conversions and H_2 yields above the traditional equilibrium values. Pd-based membranes were shown to have high H_2 selectivity and permeability, but suffer from CO and H_2S poisoning as well as prohibitive costs. In contrast, silica-based membranes appear to be devoid of all the drawbacks associated with Pd membranes, but their

hydrothermal stability must be improved to allow long-term operation. Zeolite-based membranes exhibit promising H_2 permeability owing to their ordered structures; however, the existence of intercrystalline gaps in the material results in poorer H_2 selectivity. Carbon-based membranes have been reported to be effective at removing H_2 during organic compound decomposition but their application is currently limited to non-oxidising environments. Their selectivity towards H_2 also requires improvement.

High-temperature CO_2 sorbents have also shown promise in enhanced H_2 production. CaO-based sorbents, owing to their high theoretical sorption capacity and low cost, were the most widely used material to enhance H_2 production from processes such as SMR, glycerol reforming, methanol and ethanol reforming. It is widely known that the true capture capacity of CaO-based sorbents decreases rapidly owing to product layer formation, sintering and attrition; however, the incorporation of inert supports allows these sorbents to undergo long-term cycling without serious degradation. Hydrotalcite-based sorbents were identified as a strong competitor owing to their ability to adsorb CO_2 at temperatures closer to those necessary for WGS. However, these sorbents have yet to demonstrate sufficiently-high uptake capacities. The use of alkali metal oxides as CO_2 sorbents, on the other hand, has been studied to a much lesser extent. Li_2ZrO_3 and Li_4SiO_4 have been ruled out owing to their slow sorption kinetics. Na_2ZrO_3 has shown promising results but the interaction between Na_2ZrO_3 and methane reforming catalysts has yet to be explored.

A hybrid concept whereby both H_2 membranes and CO_2 sorbents are used together in a single reactor has also been investigated. The hybrid sorbent-membrane reactor demonstrated the greatest H_2 yield, higher than both the standalone membrane and sorbent reactors. CFD simulation is a powerful tool for gaining intensive insight into reactor performance and reaction processes and can play a key role in optimising reactor design and operation.

9. Acronyms

APR	Aqueous-phase reforming
CFD	Computational fluid dynamics
CVD	Chemical vapour deposition
DFT	Density functional theory
DMDPS	Dimethoxydiphenylsilane
DMF	Dimethyl formamide
FFA	Furfuryl alcohol
GHG	Greenhouse gas
GHSV	Gas hourly space velocity
HAMR	Hybrid adsorbent-membrane reactor
HMDS	Hexamethyldisiloxane
LDH	Layered double hydroxides
LHHW	Langmuir-Hinshelwood-Hougen-Watson
MASER	Membrane-assisted sorption-enhanced reactor
MASMR	Membrane-assisted steam methane reforming
MOF	Metal organic framework
PAN	Polyacrylonitrile
PEG	Polyethylene glycol
PFA	Polyfurfuryl alcohol
PFNR	Phenol formaldehyde novolac resin
PSA	Pressure-swing adsorption
PVDC-AC	Polyvinylidenechloride-acrylate terpolymer
SEMR	Sorption-enhanced membrane reactor
TEOS	Tetraethoxysilane
TMOS	Tetramethoxysilane
WGS	Water-gas-shift
WHSV	Weight hourly space velocity

Conflicts of interest

There are no conflicts to declare

Acknowledgements

This work was supported by the National Natural Science Foundation of China (grant number: 51506112) and Tsinghua University Initiative Scientific Research Program (grant number: 20161080094). G. Ji is grateful for the financial support from China Postdoctoral Science Foundation (grant number: 2017M610910) and International Postdoctoral Exchange Fellowship Program. JY, PSF, PTC and EJA would like to thank the EPSRC and UKCCSRC for financial support through grant number EP/P026214/1.

Notes and references

1. Y. Kalinci, A. Hepbasli and I. Dincer, *Int. J. Hydrogen Energy*, 2009, **34**, 8799-8817.
2. R. M. Navarro, M. C. Sanchez-Sanchez, M. C. Alvarez-Galvan, F. d. Valle and J. L. G. Fierro, *Energy. Environ. Sci.*, 2009, **2**, 35-54.
3. P. M. Mortensen, J. D. Grunwaldt, P. A. Jensen, K. G. Knudsen and A. D. Jensen, *Appl Catal A-Gen*, 2011, **407**, 1-19.
4. G. Marnellos and M. Stoukides, *Science*, 1998, **282**, 98-100.
5. G. Q. Lu, J. C. Diniz da Costa, M. Duke, S. Giessler, R. Socolow, R. H. Williams and T. Kreutz, *J. Colloid Interface Sci.*, 2007, **314**, 589-603.
6. R. F. Service, *Science*, 2009, **324**, 1257-1259.
7. N. Armaroli and V. Balzani, *Energy. Environ. Sci.*, 2011, **4**, 3193-3222.
8. A. Hawkes, I. Staffell, D. Brett and N. Brandon, *Energy. Environ. Sci.*, 2009, **2**, 729-744.
9. A. Sternberg and A. Bardow, *Energy. Environ. Sci.*, 2015, **8**, 389-400.
10. M. Nagao, M. Takahashi and T. Hibino, *Energy. Environ. Sci.*, 2010, **3**, 1934-1940.
11. R. F. Service, *Science*, 1999, **285**, 682-685.
12. Y. Chen, Y. Wang, H. Xu and G. Xiong, *Appl. Catal. B-Environ*, 2008, **81**, 283-294.
13. D. A. Bell, B. F. Towler and M. Fan, *Coal Gasification and Its Applications*, Elsevier Science, 2010.
14. S. Smart, C. X. C. Lin, L. Ding, K. Thambimuthu and J. C. Diniz da Costa, *Energy. Environ. Sci.*, 2010, **3**, 268-278.
15. C. Dang, H. Wang, H. Yu and F. Peng, *Appl Catal A-Gen*, 2017, **533**, 9-16.
16. B. Dou, V. Dupont, P. T. Williams, H. Chen and Y. Ding, *Bioresour. Technol.*, 2009, **100**, 2613-2620.
17. X. Wang, M. Li, S. Li, H. Wang, S. Wang and X. Ma, *Fuel Process. Technol.*, 2010, **91**, 1812-1818.
18. A. C. D. Freitas and R. Guirardello, *Int. J. Hydrogen Energy*, 2014, **39**, 17969-17984.
19. P. D. Vaidya and A. E. Rodrigues, *Chem. Eng. Technol.*, 2009, **32**, 1463-1469.
20. Y.-C. Lin, *Int. J. Hydrogen Energy*, 2013, **38**, 2678-2700.
21. M. Shokrollahi Yancheshmeh, H. R. Radfarnia and M. C. Iliuta, *Chem. Eng. J.*, 2016, **283**, 420-444.
22. M. Bayat, Z. Dehghani and M. R. Rahimpour, *Journal of Industrial and Engineering Chemistry*, 2014, **20**, 3256-3269.
23. A. Haryanto, S. Fernando, N. Murali and S. Adhikari, *Energ. Fuel.*, 2005, **19**, 2098-2106.
24. M. C. Sánchez-Sánchez, R. M. Navarro and J. L. G. Fierro, *Int. J. Hydrogen Energy*, 2007, **32**, 1462-1471.
25. N. Laosiripojana and S. Assabumrungrat, *J. Power Sources*, 2007, **163**, 943-951.
26. N. Homs, J. Llorca and P. R. de la Piscina, *Catal. Today*, 2006, **116**, 361-366.
27. Y.-M. Lin and M.-H. Rei, *Catal. Today*, 2001, **67**, 77-84.
28. A. Z'Graggen, P. Haueter, D. Trommer, M. Romero, J. C. de Jesus and A. Steinfeld, *Int. J. Hydrogen Energy*, 2006, **31**, 797-811.
29. T. Davidian, N. Guilhaume, E. Iojoiu, H. Provendier and C. Mirodatos, *Appl. Catal. B-Environ*, 2007, **73**, 116-127.
30. S. Turn, C. Kinoshita, Z. Zhang, D. Ishimura and J. Zhou, *Int. J. Hydrogen Energy*, 1998, **23**, 641-648.
31. F. Chen, C. Wu, L. Dong, A. Vassallo, P. T. Williams and J. Huang, *Appl. Catal. B-Environ*, 2016, **183**, 168-175.
32. M. Balat and M. Balat, *Int. J. Hydrogen Energy*, 2009, **34**, 3589-3603.
33. R. D. Cortright, R. R. Davda and J. A. Dumesic, *Nature*, 2002, **418**, 964-967.
34. P. Ji, W. Feng and B. Chen, *Chem. Eng. Sci.*, 2009, **64**, 582-592.
35. A. Tanksale, J. N. Beltramini and G. M. Lu, *Renew. Sust. Energ. Rev.*, 2010, **14**, 166-182.
36. R. C. Saxena, D. Seal, S. Kumar and H. B. Goyal, *Renew. Sust. Energ. Rev.*, 2008, **12**, 1909-1927.
37. L. Meng and T. Tsuru, *Catal. Today*, 2016, **268**, 3-11.
38. S. Battersby, P. W. Teixeira, J. Beltramini, M. C. Duke, V. Rudolph and J. C. Diniz da Costa, *Catal. Today*, 2006, **116**, 12-17.
39. M. Nomura, S. Kasahara and S.-i. Nakao, *Ind. Eng. Chem. Res.*, 2004, **43**, 5874-5879.
40. C.-I. Ahn, D.-W. Jeong, J. M. Cho, H.-S. Na, W.-J. Jang, H.-S. Roh, J.-H. Choi, S. H. Um and J. W. Bae, *Microporous Mesoporous Mater.*, 2016, **221**, 204-211.
41. T. L. LeValley, A. R. Richard and M. Fan, *Int. J. Hydrogen Energy*, 2014, **39**, 16983-17000.
42. R. Smith, M. Loganathan and M. S. Shantha, *International Journal of Chemical Reactor Engineering*, 2010, **8**.
43. Z. Sun, W. Xiang and S. Chen, *Int. J. Hydrogen Energy*, 2016, **41**, 17323-17333.

44. C. A. Scholes, K. H. Smith, S. E. Kentish and G. W. Stevens, *Int J Green Gas Con*, 2010, **4**, 739-755.
45. K. Akamatsu, T. Murakami, T. Sugawara, R. Kikuchi and S.-i. Nakao, *AlChE J.*, 2011, **57**, 1882-1888.
46. B. Deonarine, G. Ji, S. Smart, J. C. D. D. Costa, G. Reed and M. Millan, *Fuel Process. Technol.*, 2016.
47. J. Xu and G. F. Froment, *AlChE J.*, 1989, **35**, 97-103.
48. A. Iulianelli, S. Liguori, J. Wilcox and A. Basile, *Catal Rev*, 2016, **58**, 1-35.
49. C. S. Patil, M. van Sint Annaland and J. A. M. Kuipers, *Chem. Eng. Sci.*, 2007, **62**, 2989-3007.
50. B. Dittmar, A. Behrens, N. Schödel, M. Rüttinger, T. Franco, G. Straczewski and R. Dittmeyer, *Int. J. Hydrogen Energy*, 2013, **38**, 8759-8771.
51. C.-H. Kim, J.-Y. Han, H. Lim, D.-W. Kim and S.-K. Ryi, *Korean J. Chem. Eng.*, 2017, **34**, 1260-1265.
52. R. Khonde and A. Chaurasia, *Int. J. Hydrogen Energy*, 2016, **41**, 8793-8802.
53. N. H. Florin and A. T. Harris, *AlChE J.*, 2008, **54**, 1096-1109.
54. X. Zhao, H. Zhou, V. S. Sikarwar, M. Zhao, A.-H. A. Park, P. S. Fennell, L. Shen and L.-S. Fan, *Energy. Environ. Sci.*, 2017, DOI: 10.1039/C6EE03718F.
55. T. Utaka, K. Sekizawa and K. Eguchi, *Appl Catal A-Gen*, 2000, **194-195**, 21-26.
56. M. J. L. Ginés, N. Amadeo, M. Laborde and C. R. Apesteguía, *Appl Catal A-Gen*, 1995, **131**, 283-296.
57. S. Sircar and T. C. Golden, *Sep. Sci. Technol.*, 2000, **35**, 667-687.
58. A. Mahecha-Botero, T. Boyd, A. Gulamhusein, N. Comyn, C. J. Lim, J. R. Grace, Y. Shirasaki and I. Yasuda, *Chem. Eng. Sci.*, 2008, **63**, 2752-2762.
59. M. Hu, D. Guo, C. Ma, Z. Hu, B. Zhang, B. Xiao, S. Luo and J. Wang, *Energy*, 2015, **90, Part 1**, 857-863.
60. R. Espinal, A. Anzola, E. Adrover, M. Roig, R. Chimentao, F. Medina, E. López, D. Borio and J. Llorca, *Int. J. Hydrogen Energy*, 2014, **39**, 10902-10910.
61. S. J. Han, J. H. Song, J. Yoo, S. Park, K. H. Kang and I. K. Song, *Int. J. Hydrogen Energy*, 2017, **42**, 5886-5898.
62. R. Hu, D. Li, H. Xue, N. Zhang, Z. Liu and Z. Liu, *Int. J. Hydrogen Energy*, 2017, **42**, 7786-7797.
63. H. Xie, Q. Yu, Z. Zuo, Z. Han, X. Yao and Q. Qin, *Int. J. Hydrogen Energy*, 2016, **41**, 2345-2353.
64. S. Rönsch, J. Köchermann, J. Schneider and S. Matthischke, *Chem. Eng. Technol.*, 2016, **39**, 208-218.
65. J. W. Snoeck, G. F. Froment and M. Fowles, *Ind. Eng. Chem. Res.*, 2002, **41**, 4252-4265.
66. C. C. Sreejith, C. Muraleedharan and P. Arun, *Fuel Process. Technol.*, 2015, **130**, 197-207.
67. J. Xu and G. F. Froment, *AlChE J.*, 1989, **35**, 88-96.
68. Y. Wang and C. M. Kinoshita, *Solar Energy*, 1993, **51**, 19-25.
69. N. D. Couto, V. B. Silva and A. Rouboa, *Journal of Cleaner Production*, 2016, **139**, 622-635.
70. L. Barelli, G. Bidini, F. Gallorini and S. Servili, *Energy*, 2008, **33**, 554-570.
71. A. Julbe, D. Farrusseng and C. Guizard, *J Membrane Sci*, 2001, **181**, 3-20.
72. G. Saracco, H. W. J. P. Neomagus, G. F. Versteeg and W. P. M. v. Swaaij, *Chem. Eng. Sci.*, 1999, **54**, 1997-2017.
73. G. Barbieri, A. Brunetti, T. Granato, P. Bernardo and E. Drioli, *Ind. Eng. Chem. Res.*, 2005, **44**, 7676-7683.
74. B. T. Carvill, J. R. Hufton, M. Anand and S. Sircar, *AlChE J.*, 1996, **42**, 2765-2772.
75. Q. Zhang, D. Han, Y. Liu, Q. Ye and Z. Zhu, *AlChE J.*, 2013, **59**, 901-911.
76. E. Ochoa-Fernández, H. K. Rusten, H. A. Jakobsen, M. Rønning, A. Holmen and D. Chen, *Catal. Today*, 2005, **106**, 41-46.
77. N. W. Ockwig and T. M. Nenoff, *Chem. Rev.*, 2007, **107**, 4078-4110.
78. Z. Kang, M. Xue, L. Fan, L. Huang, L. Guo, G. Wei, B. Chen and S. Qiu, *Energy. Environ. Sci.*, 2014, **7**, 4053-4060.
79. D. Uhlmann, S. Smart and J. C. Diniz da Costa, *Sep. Purif. Technol.*, 2010, **76**, 171-178.
80. C. R. Miller, D. K. Wang, S. Smart and J. C. Diniz da Costa, *Sci. Rep.*, 2013, **3**, 1-6.
81. D. Uhlmann, S. Liu, B. P. Ladewig and J. C. Diniz da Costa, *J Membrane Sci*, 2009, **326**, 316-321.
82. S. Gopalakrishnan and J. C. Diniz da Costa, *J Membrane Sci*, 2008, **323**, 144-147.
83. M. C. Duke, J. C. Diniz da Costa, G. Q. Lu, M. Petch and P. Gray, *J Membrane Sci*, 2004, **241**, 325-333.
84. J. C. Diniz da Costa, G. Q. Lu, V. Rudolph and Y. S. Lin, *J Membrane Sci*, 2002, **198**, 9-21.
85. S. Smart, J. F. Vente and J. C. Diniz da Costa, *Int. J. Hydrogen Energy*, 2012, **37**, 12700-12707.
86. G. Ji, G. Wang, K. Hooman, S. Bhatia and J. C. Diniz da Costa, *Chem. Eng. Sci.*, 2014, **111**, 142-152.
87. S. Yun and S. Ted Oyama, *J Membrane Sci*, 2011, **375**, 28-45.
88. F. A. Lewis, *Platinum Met. Rev.*, 1982, **26**, 121-128.
89. B. Cordero, V. Gomez, A. E. Platero-Prats, M. Reves, J. Echeverria, E. Cremades, F. Barragan and S. Alvarez, *Dalton Transactions*, 2008, DOI: 10.1039/B801115J, 2832-2838.
90. G. L. Holleck, *The Journal of Physical Chemistry*, 1970, **74**, 503-511.
91. A. Li, W. Liang and R. Hughes, *J Membrane Sci*, 2000, **165**, 135-141.
92. B. D. Morreale, M. V. Ciocco, R. M. Enick, B. I. Morsi, B. H. Howard, A. V. Cugini and K. S. Rothenberger, *J Membrane Sci*, 2003, **212**, 87-97.
93. W.-H. Chen, W.-Z. Syu, C.-I. Hung, Y.-L. Lin and C.-C. Yang, *Int. J. Hydrogen Energy*, 2012, **37**, 12666-12679.
94. E. Fernandez, K. Coenen, A. Helmi, J. Melendez, J. Zuñiga, D. A. Pacheco Tanaka, M. van Sint Annaland and F. Gallucci, *Int. J. Hydrogen Energy*, 2015, **40**, 13463-13478.
95. J. Boon, J. A. Z. Pieterse, F. P. F. van Berkel, Y. C. van Delft and M. van Sint Annaland, *J Membrane Sci*, 2015, **496**, 344-358.
96. W.-H. Chen, C.-H. Lin and Y.-L. Lin, *J Membrane Sci*, 2014, **472**, 45-54.
97. G. Ji and M. Zhao, in *Recent Advances in Carbon Capture and Storage*, ed. Y. Yun, InTech, Rijeka, 2017, DOI: 10.5772/65723, p. Ch. 03.

98. B. K. R. Nair, J. Choi and M. P. Harold, *J Membrane Sci*, 2007, **288**, 67-84.
99. S. Q. Hao and D. S. Sholl, *Energy. Environ. Sci.*, 2008, **1**, 175-183.
100. A. S. Augustine, M. E. Ayturk, N. Kazantzis and Y. H. Ma, 2009.
101. S. Uemiya, N. Sato, H. Ando and E. Kikuchi, *Ind. Eng. Chem. Res.*, 1991, **30**, 585-589.
102. E. Fernandez, A. Helmi, J. A. Medrano, K. Coenen, A. Arratibel, J. Melendez, N. C. A. de Nooijer, V. Spallina, J. L. Viviente, J. Zuñiga, M. van Sint Annaland, D. A. Pacheco Tanaka and F. Gallucci, *Int. J. Hydrogen Energy*, 2017.
103. F. Gallucci, F. Chiaravalloti, S. Tosti, E. Drioli and A. Basile, *Int. J. Hydrogen Energy*, 2007, **32**, 1837-1845.
104. Y. Sakamoto, F. L. Chen, Y. Kinari and F. Sakamoto, *Int. J. Hydrogen Energy*, 1996, **21**, 1017-1024.
105. H. Lim, Y. Gu and S. T. Oyama, *J Membrane Sci*, 2012, **396**, 119-127.
106. S. Uemiya, N. Sato, H. Ando, T. Matsuda and E. Kikuchi, *J. Jpn. Pet. Inst*, 1990, **33**, 418-421.
107. K. Ohira, Y. Sakamoto and T. B. Flanagan, *J. Alloys Compd.*, 1996, **236**, 42-49.
108. J. Shu, B. P. A. Grandjean and S. Kaliaguine, *Appl Catal A-Gen*, 1994, **119**, 305-325.
109. K. Ghasemzadeh, S. Liguori, P. Morrone, A. Iulianelli, V. Piemonte, A. A. Babaluo and A. Basile, *Int. J. Hydrogen Energy*, 2013, **38**, 16685-16697.
110. W.-H. Chen, M.-H. Hsia, Y.-H. Chi, Y.-L. Lin and C.-C. Yang, *Appl. Energ.*, 2014, **113**, 41-50.
111. W.-H. Chen and P.-C. Hsu, *Int. J. Hydrogen Energy*, 2011, **36**, 9355-9366.
112. P. Kamakoti and D. S. Sholl, *J Membrane Sci*, 2003, **225**, 145-154.
113. L. Semidey-Flecha, C. Ling and D. S. Sholl, *J Membrane Sci*, 2010, **362**, 384-392.
114. S. Yun, H. Lim and S. Ted Oyama, *J Membrane Sci*, 2012, **409–410**, 222-231.
115. H. W. Abu El Hawa, S.-T. B. Lundin, N. S. Patki and J. Douglas Way, *Int. J. Hydrogen Energy*, 2016, **41**, 10193-10201.
116. L. Wang, R. Yoshiie and S. Uemiya, *J Membrane Sci*, 2007, **306**, 1–7.
117. S. W. Nam, S. P. Yoon, H. Y. Ha, S.-A. Hong and A. P. Maganyuk, *Korean J. Chem. Eng.*, 2000, **17**, 288-291.
118. H. W. Abu El Hawa, S. N. Paglieri, C. C. Morris, A. Harale and J. Douglas Way, *Sep. Purif. Technol.*, 2015, **147**, 388-397.
119. Y. S. Cheng, M. A. Peña, J. L. Fierro, D. C. W. Hui and K. L. Yeung, *J Membrane Sci*, 2002, **204**, 329-340.
120. F. Gallucci, E. Fernandez, P. Corengia and M. van Sint Annaland, *Chem. Eng. Sci.*, 2013, **92**, 40-66.
121. P. Kamakoti and D. S. Sholl, *J Membrane Sci*, 2006, **279**, 94-99.
122. S. H. D. Lee, D. V. Applegate, S. Ahmed, S. G. Calderone and T. L. Harvey, *Int. J. Hydrogen Energy*, 2005, **30**, 829-842.
123. J. Martinez-Frias, A.-Q. Pham and S. M. Aceves, *Int. J. Hydrogen Energy*, 2003, **28**, 483-490.
124. B. Anzelmo, J. Wilcox and S. Liguori, *J Membrane Sci*, 2017, **522**, 343-350.
125. A. Heinzel, B. Vogel and P. Hübner, *J. Power Sources*, 2002, **105**, 202-207.
126. J. Zhang, D. Liu, M. He, H. Xu and W. Li, *J Membrane Sci*, 2006, **274**, 83-91.
127. J. M. Sánchez, M. M. Barreiro and M. Maroño, *Fuel*, 2014, **116**, 894-903.
128. K. Hou and R. Hughes, *Chem. Eng. J.*, 2001, **82**, 311-328.
129. J. Tong and Y. Matsumura, *Appl Catal A-Gen*, 2005, **286**, 226-231.
130. M. Sarić, Y. C. van Delft, R. Sumbharaju, D. F. Meyer and A. de Groot, *Catal. Today*, 2012, **193**, 74-80.
131. L. Roses, F. Gallucci, G. Manzolini and M. van Sint Annaland, *Chem. Eng. J.*, 2013, **222**, 307-320.
132. Y. Bi, H. Xu, W. Li and A. Goldbach, *Int. J. Hydrogen Energy*, 2009, **34**, 2965-2971.
133. R. Sanz, J. A. Calles, D. Alique and L. Furones, *Int. J. Hydrogen Energy*, 2014, **39**, 4739-4748.
134. M. Matsuka, M. Higashi and T. Ishihara, *Int. J. Hydrogen Energy*, 2013, **38**, 6673-6680.
135. M. Patrascu and M. Sheintuch, *Chem. Eng. J.*, 2015, **262**, 862-874.
136. J. Tong and Y. Matsumura, *Catal. Today*, 2006, **111**, 147-152.
137. J. Tong, Y. Matsumura, H. Suda and K. Haraya, *Ind. Eng. Chem. Res.*, 2005, **44**, 1454-1465.
138. T. Kume, Y. Ikeda, T. Iseki, H. Yakabe, H. Tanaka, H. Hikosaka, Y. Takagi and M. Ito, *Int. J. Hydrogen Energy*, 2013, **38**, 6079-6084.
139. Y. Matsumura and J. Tong, *Top. Catal.*, 2008, **51**, 123-132.
140. F. Gallucci, L. Paturzo, A. Famà and A. Basile, *Ind. Eng. Chem. Res.*, 2004, **43**, 928-933.
141. Y. Shirasaki, T. Tsuneki, Y. Ota, I. Yasuda, S. Tachibana, H. Nakajima and K. Kobayashi, *Int. J. Hydrogen Energy*, 2009, **34**, 4482-4487.
142. J. A. Medrano, E. Fernandez, J. Melendez, M. Parco, D. A. P. Tanaka, M. van Sint Annaland and F. Gallucci, *Int. J. Hydrogen Energy*, 2016, **41**, 8706-8718.
143. F. S. A. Silva, M. Benachour and C. A. M. Abreu, *Brazilian Journal of Chemical Engineering*, 2015, **32**, 201-210.
144. S. Liguori, A. Iulianelli, F. Dalena, V. Piemonte, Y. Huang and A. Basile, *Int. J. Hydrogen Energy*, 2014, **39**, 18702-18710.
145. C. Mateos-Pedrero, H. Silva, D. A. Pacheco Tanaka, S. Liguori, A. Iulianelli, A. Basile and A. Mendes, *Appl. Catal. B-Environ*, 2015, **174–175**, 67-76.
146. F. R. García-García, S. C. Tsang and K. Li, *J Membrane Sci*, 2014, **455**, 92-102.
147. M. A. Islam and S. Ilias, *Sep. Sci. Technol.*, 2012, **47**, 2177-2185.
148. A. M. da Silva, L. V. Mattos, J. Múnera, E. Lombardo, F. B. Noronha and L. Cornaglia, *Int. J. Hydrogen Energy*, 2015, **40**, 4154-4166.
149. M. Domínguez, E. Taboada, E. Molins and J. Llorca, *Catal. Today*, 2012, **193**, 101-106.
150. A. Iulianelli and A. Basile, *Int. J. Hydrogen Energy*, 2010, **35**, 3170-3177.
151. A. Iulianelli, S. Liguori, T. Longo, S. Tosti, P. Pinacci and A. Basile, *Int. J. Hydrogen Energy*, 2010, **35**, 3159-3164.

152. P. K. Seelam, S. Liguori, A. Iulianelli, P. Pinacci, V. Calabrò, M. Huuhtanen, R. Keiski, V. Piemonte, S. Tosti, M. De Falco and A. Basile, *Catal. Today*, 2012, **193**, 42-48.
153. M. A. Murmura, M. Patrascu, M. C. Annesini, V. Palma, C. Ruocco and M. Sheintuch, *Int. J. Hydrogen Energy*, 2015, **40**, 5837-5848.
154. A. Iulianelli, S. Liguori, A. Vita, C. Italiano, C. Fabiano, Y. Huang and A. Basile, *Catal. Today*, 2016, **259, Part 2**, 368-375.
155. E. López, N. J. Divins and J. Llorca, *Catal. Today*, 2012, **193**, 145-150.
156. A. Hedayati, O. Le Corre, B. Lacarrière and J. Llorca, *Catal. Today*, 2016, **268**, 68-78.
157. E. Y. Mironova, M. M. Ermilova, N. V. Orekhova, D. N. Muraviev and A. B. Yaroslavtsev, *Catal. Today*, 2014, **236, Part A**, 64-69.
158. S. F. Wu and L. L. Wang, *Int. J. Hydrogen Energy*, 2010, **35**, 6518-6524.
159. A. Gouveia Gil, Z. Wu, D. Chadwick and K. Li, *Appl Catal A-Gen*, 2015, **506**, 188-196.
160. A. Arratibel Plazaola, D. Pacheco Tanaka, M. Van Sint Annaland and F. Gallucci, *Molecules*, 2017, **22**, 51.
161. Y. Zhang, J. Gwak, Y. Murakoshi, T. Ikehara, R. Maeda and C. Nishimura, *J Membrane Sci*, 2006, **277**, 203-209.
162. J. Boon, V. Spallina, Y. van Delft and M. van Sint Annaland, *Int J Green Gas Con*, 2016, **50**, 121-134.
163. P. Prasad and S. S. E. H. Elnashaie, *Ind. Eng. Chem. Res.*, 2004, **43**, 494-501.
164. P. Prasad and S. S. E. H. Elnashaie, *Ind. Eng. Chem. Res.*, 2003, **42**, 4715-4722.
165. A. M. Adris, C. J. Lim and J. R. Grace, *Chem. Eng. Sci.*, 1997, **52**, 1609-1622.
166. A.-E. M. Adris, Text, 1994.
167. Z. Chen, Y. Yan and S. S. E. H. Elnashaie, *Chem. Eng. Sci.*, 2003, **58**, 4335-4349.
168. Z. Chen, J. R. Grace, C. Jim Lim and A. Li, *Int. J. Hydrogen Energy*, 2007, **32**, 2359-2366.
169. K. Ghasemzadeh, A. Aghaeinejad-Meybodi, M. J. Vaezi, A. Gholizadeh, M. A. Abdi, A. A. Babaluo, M. Haghighi and A. Basile, *RSC Adv.*, 2015, **5**, 95823-95832.
170. K. Ghasemzadeh, P. Morrone, A. A. Babalou and A. Basile, *Int. J. Hydrogen Energy*, 2015, **40**, 3909-3918.
171. D. R. Palo, R. A. Dagle and J. D. Holladay, *Chem. Rev.*, 2007, **107**, 3992-4021.
172. G. A. Deluga, J. R. Salge, L. D. Schmidt and X. E. Verykios, *Science*, 2004, **303**, 993-997.
173. M. Coroneo, G. Montante, J. Catalano and A. Paglianti, *J Membrane Sci*, 2009, **343**, 34-41.
174. C. Yacou, S. Smart and J. C. Diniz da Costa, *Energy. Environ. Sci.*, 2012, **5**, 5820-5832.
175. M. Duke, V. Rudolph, G. Q. Lu and J. C. Diniz da Costa, *AlChE J.*, 2004, **50**, 2630-2634.
176. K. Akamatsu, M. Nakane, T. Sugawara, T. Hattori and S.-i. Nakao, *J Membrane Sci*, 2008, **325**, 16-19.
177. K. Akamatsu, Y. Ohta, T. Sugawara, T. Hattori and S.-i. Nakao, *Ind. Eng. Chem. Res.*, 2008, **47**, 9842-9847.
178. J. C. D. Da Costa, G. Q. Lu, H. Y. Zhu and V. Rudolph, *J. Porous Mater.*, 1999, **6**, 143-151.
179. S. Qiu, M. Xue and G. Zhu, *Chem. Soc. Rev.*, 2014, **43**, 6116-6140.
180. S. Battersby, T. Tasaki, S. Smart, B. Ladewig, S. Liu, M. C. Duke, V. Rudolph and J. C. Diniz da Costa, *J Membrane Sci*, 2009, **329**, 91-98.
181. B. Ballinger, J. Motuzas, S. Smart and J. C. Diniz da Costa, *J Membrane Sci*, 2014, **451**, 185-191.
182. M. C. Duke, J. C. Diniz da Costa, G. Q. Lu and P. G. Gray, *AlChE J.*, 2006, **52**, 1729-1735.
183. T. Tsuru, K. Yamaguchi, T. Yoshioka and M. Asaeda, *AlChE J.*, 2004, **50**, 2794-2805.
184. T. Tsuru, T. Morita, H. Shintani, T. Yoshioka and M. Asaeda, *J Membrane Sci*, 2008, **316**, 53-62.
185. T. A. Peters, M. Stange, H. Klette and R. Bredesen, *J Membrane Sci*, 2008, **316**, 119-127.
186. S. Giessler, L. Jordan, J. C. D. D. Costa and G. Q. Lu, *Separation & Purification Technology*, 2003, **32**, 255-264.
187. A. Brunetti, G. Barbieri, E. Drioli, K. H. Lee, B. Sea and D. W. Lee, *Chem. Eng. Process.*, 2007, **46**, 119-126.
188. S. Battersby, M. C. Duke, S. Liu, V. Rudolph and J. C. D. d. Costa, *J Membrane Sci*, 2008, **316**, 46-52.
189. A. Brunetti, G. Barbieri, E. Drioli, T. Granato and K. H. Lee, *Chem. Eng. Sci.*, 2007, **62**, 5621-5626.
190. S. Araki, H. Miyanishi, H. Yano, S. Tanaka and Y. Miyake, *Sep. Sci. Technol.*, 2013, **48**, 76-83.
191. S. E. Battersby, D. Miller, M. Zed, J. Patch, V. Rudolph, M. C. Duke and J. C. Diniz da Costa, *Advances in Applied Ceramics*, 2007, **106**, 29-34.
192. S. Battersby, B. P. Ladewig, M. Duke, V. Rudolph and J. C. Diniz da Costa, *Asia-Pac J Chem Eng*, 2010, **5**, 83-92.
193. G. Li, M. Kanezashi, H. R. Lee, M. Maeda, T. Yoshioka and T. Tsuru, *Int. J. Hydrogen Energy*, 2012, **37**, 12105-12113.
194. G. Li, M. Kanezashi, T. Yoshioka and T. Tsuru, *AlChE J.*, 2013, **59**, 168-179.
195. D.-W. Lee, S.-J. Park, C.-Y. Yu, S.-K. Ihm and K.-H. Lee, *J Membrane Sci*, 2008, **316**, 63-72.
196. L. Wei and K. Kawamoto, *Chem. Eng. Technol.*, 2013, **36**, 650-656.
197. T. Tsuru, *J. Jpn. Pet. Inst*, 2011, **54**, 277-286.
198. K. Oda, K. Akamatsu, T. Sugawara, R. Kikuchi, A. Segawa and S.-i. Nakao, *Ind. Eng. Chem. Res.*, 2010, **49**, 11287-11293.
199. G. Li, K. Yada, M. Kanezashi, T. Yoshioka and T. Tsuru, *Ind. Eng. Chem. Res.*, 2013, **52**, 13325-13332.
200. L. Meng, X. Yu, T. Niimi, H. Nagasawa, M. Kanezashi, T. Yoshioka and T. Tsuru, *AlChE J.*, 2015, **61**, 1628-1638.
201. K. Akamatsu, T. Tago, M. Seshimo and S.-i. Nakao, *Ind. Eng. Chem. Res.*, 2015, **54**, 3996-4000.
202. K. Akamatsu, Y. Ohta, T. Sugawara, N. Kanno, K. Tonokura, T. Hattori and S.-i. Nakao, *J Membrane Sci*, 2009, **330**, 1-4.
203. H. Lim, Y. Gu and S. T. Oyama, *J Membrane Sci*, 2010, **351**, 149-159.
204. M. C. Duke, J. C. D. da Costa, D. D. Do, P. G. Gray and G. Q. Lu, *Adv. Funct. Mater.*, 2006, **16**, 1215-1220.
205. R. Igi, T. Yoshioka, Y. H. Ikuhara, Y. Iwamoto and T. Tsuru, *J. Am. Ceram. Soc.*, 2008, **91**, 2975-2981.
206. C. M. Kinoshita and S. Q. Turn, *Int. J. Hydrogen Energy*, 2003, **28**, 1065-1071.
207. S. Sarkar and A. Kumar, *Bioresour. Technol.*, 2010, **101**, 7350-7361.

208. G. J. Stiegel and M. Ramezan, *Int. J. Coal Geol*, 2006, **65**, 173-190.
209. H. Jin, Y. Lu, B. Liao, L. Guo and X. Zhang, *Int. J. Hydrogen Energy*, 2010, **35**, 7151-7160.
210. S. Battersby, M. C. Duke, S. Liu, V. Rudolph and J. C. D. d. Costa, *J Membrane Sci*, 2008, **316**, 46-52.
211. S. Battersby, S. Smart, B. Ladewig, S. Liu, M. C. Duke, V. Rudolph and J. C. D. d. Costa, *Sep. Purif. Technol.*, 2009, **66**, 299-305.
212. L. Liu, D. K. Wang, D. L. Martens, S. Smart and J. C. Diniz da Costa, *J Membrane Sci*, 2015, **475**, 425-432.
213. M. Kanezashi and M. Asaeda, *J Membrane Sci*, 2006, **271**, 86-93.
214. V. Boffa, J. E. ten Elshof, A. V. Petukhov and D. H. A. Blank, *ChemSusChem*, 2008, **1**, 437-443.
215. V. Boffa, D. H. A. Blank and J. E. ten Elshof, *J Membrane Sci*, 2008, **319**, 256-263.
216. H. Qi, H. Chen, L. Li, G. Zhu and N. Xu, *J Membrane Sci*, 2012, **421-422**, 190-200.
217. M. E. Davis, *Nature*, 2002, **417**, 813-821.
218. J. Xiao and J. Wei, *Chem. Eng. Sci.*, 1992, **47**, 1123-1141.
219. J. Xiao and J. Wei, *Chem. Eng. Sci.*, 1992, **47**, 1143-1159.
220. U. Illgen, R. Schäfer, M. Noack, P. Kölsch, A. Kühnle and J. Caro, *Catal. Commun.*, 2001, **2**, 339-345.
221. B. S. Liu and C. T. Au, *Catal. Lett.*, 2001, **77**, 67-74.
222. B.-H. Jeong, K.-I. Sotowa and K. Kusakabe, *J Membrane Sci*, 2003, **224**, 151-158.
223. Y. Zhang, Z. Wu, Z. Hong, X. Gu and N. Xu, *Chem. Eng. J.*, 2012, **197**, 314-321.
224. X. Dong, H. Wang, Z. Rui and Y. S. Lin, *Chem. Eng. J.*, 2015, **268**, 219-229.
225. Z. Tang, S.-J. Kim, G. K. Reddy, J. Dong and P. Smirniotis, *J Membrane Sci*, 2010, **354**, 114-122.
226. S.-J. Kim, Z. Xu, G. K. Reddy, P. Smirniotis and J. Dong, *Ind. Eng. Chem. Res.*, 2012, **51**, 1364-1375.
227. N. Rangnekar, N. Mittal, B. Elyassi, J. Caro and M. Tsapatsis, *Chem. Soc. Rev.*, 2015, **44**, 7128-7154.
228. H. Bux, A. Feldhoff, J. Cravillon, M. Wiebcke, Y.-S. Li and J. Caro, *Chem. Mater.*, 2011, **23**, 2262-2269.
229. S.-R. Lee, Y.-H. Son, A. Julbe and J.-H. Choy, *Thin Solid Films*, 2006, **495**, 92-96.
230. J. Motuzas, A. Julbe, R. D. Noble, C. Guizard, Z. J. Beresnevicius and D. Cot, *Microporous Mesoporous Mater.*, 2005, **80**, 73-83.
231. M. Pan and Y. S. Lin, *Microporous Mesoporous Mater.*, 2001, **43**, 319-327.
232. X. Dong, K. Huang, S. Liu, R. Ren, W. Jin and Y. S. Lin, *J. Mater. Chem.*, 2012, **22**, 19222-19227.
233. Z. Hong, C. Zhang, X. Gu, W. Jin and N. Xu, *J Membrane Sci*, 2011, **366**, 427-435.
234. D. R. Paul, *Science*, 2012, **335**, 413-414.
235. V. C. Geiszler and W. J. Koros, *Ind. Eng. Chem. Res.*, 1996, **35**, 2999-3003.
236. S. M. Saufi and A. F. Ismail, *Carbon*, 2004, **42**, 241-259.
237. Y. Song, D. K. Wang, G. Birkett, W. Martens, M. C. Duke, S. Smart and J. C. Diniz da Costa, *Journal*, 2016, **6**, 30703.
238. C. Song, T. Wang, X. Wang, J. Qiu and Y. Cao, *Sep. Purif. Technol.*, 2008, **58**, 412-418.
239. W. Wei, G. Qin, H. Hu, L. You and G. Chen, *J Membrane Sci*, 2007, **303**, 80-85.
240. J. A. Lie and M.-B. Hägg, *Carbon*, 2005, **43**, 2600-2607.
241. A. F. Ismail, K. C. Khulbe and T. Matsuura, 2015.
242. X. Zhang, H. Hu, Y. Zhu and S. Zhu, *Ind. Eng. Chem. Res.*, 2006, **45**, 7997-8001.
243. J. Agrell, M. Boutonnet and J. L. G. Fierro, *Appl Catal A-Gen*, 2003, **253**, 213-223.
244. S. Sá, J. M. Sousa and A. Mendes, *Chem. Eng. Sci.*, 2011, **66**, 5523-5530.
245. Y. Hirota, A. Ishikado, Y. Uchida, Y. Egashira and N. Nishiyama, *J Membrane Sci*, 2013, **440**, 134-139.
246. M. F. N. D'Angelo, V. Ordomsky, J. C. Schouten, J. van der Schaaf and T. A. Nijhuis, *ChemSusChem*, 2014, **7**, 2007-2015.
247. Q. Wang, J. Luo, Z. Zhong and A. Borgna, *Energy. Environ. Sci.*, 2011, **4**, 42-55.
248. M. E. Boot-Handford, J. C. Abanades, E. J. Anthony, M. J. Blunt, S. Brandani, N. Mac Dowell, J. R. Fernandez, M.-C. Ferrari, R. Gross, J. P. Hallett, R. S. Haszeldine, P. Heptonstall, A. Lyngfelt, Z. Makuch, E. Mangano, R. T. J. Porter, M. Pourkashanian, G. T. Rochelle, N. Shah, J. G. Yao and P. S. Fennell, *Energy. Environ. Sci.*, 2014, **7**, 130-189.
249. B. Moghtaderi, J. Zanganeh, K. Shah and H. Wu, *Energ. Fuel.*, 2012, **26**, 2046-2057.
250. G. Soukup, C. Pfeifer, A. Kreuzeder and H. Hofbauer, *Chem. Eng. Technol.*, 2009, **32**, 348-354.
251. S. Koppatz, C. Pfeifer, R. Rauch, H. Hofbauer, T. Marquard-Moellenstedt and M. Specht, *Fuel Process. Technol.*, 2009, **90**, 914-921.
252. J. Udomsirichakorn, P. Basu, P. Abdul Salam and B. Acharya, *Fuel Process. Technol.*, 2014, **127**, 7-12.
253. B. Acharya, A. Dutta and P. Basu, *Energ. Fuel.*, 2009, **23**, 5077-5083.
254. M. Xie, Z. Zhou, Y. Qi, Z. Cheng and W. Yuan, *Chem. Eng. J.*, 2012, **207–208**, 142-150.
255. M. Rydén and P. Ramos, *Fuel Process. Technol.*, 2012, **96**, 27-36.
256. I. Martínez, M. C. Romano, P. Chiesa, G. Grasa and R. Murillo, *Int. J. Hydrogen Energy*, 2013, **38**, 15180-15199.
257. S. Stendardo, L. K. Andersen and C. Herce, *Chem. Eng. J.*, 2013, **220**, 383-394.
258. R. H. Borgwardt, *Ind. Eng. Chem. Res.*, 1989, **28**, 493-500.
259. M. Zhao, J. Shi, X. Zhong, S. Tian, J. Blamey, J. Jiang and P. S. Fennell, *Energ Environ Sci*, 2014, **7**, 3291-3295.
260. N. MacDowell, N. Florin, A. Buchard, J. Hallett, A. Galindo, G. Jackson, C. S. Adjiman, C. K. Williams, N. Shah and P. Fennell, *Energy. Environ. Sci.*, 2010, **3**, 1645-1669.
261. S. K. Bhatia and D. D. Perlmutter, *AlChE J.*, 1983, **29**, 79-86.
262. D. Alvarez and J. C. Abanades, *Ind. Eng. Chem. Res.*, 2005, **44**, 5608-5615.
263. M. Zhang, Y. Peng, Y. Sun, P. Li and J. Yu, *Fuel*, 2013, **111**, 636-642.

264. L. Li, D. L. King, Z. Nie and C. Howard, *Ind. Eng. Chem. Res.*, 2009, **48**, 10604-10613.
265. C.-T. Yu and W.-C. Chen, *Powder Technol.*, 2013, **239**, 492-498.
266. F. Yan, J. Jiang, K. Li, S. Tian, Z. Liu, J. Shi, X. Chen, J. Fei and Y. Lu, *ACS Sustainable Chemistry & Engineering*, 2016, **4**, 7004-7012.
267. X. Zhang, Z. Li, Y. Peng, W. Su, X. Sun and J. Li, *Chem. Eng. J.*, 2014, **243**, 297-304.
268. C. Luo, Y. Zheng, N. Ding, Q. Wu, G. Bian and C. Zheng, *Ind. Eng. Chem. Res.*, 2010, **49**, 11778-11784.
269. S. F. Wu and Y. Q. Zhu, *Ind. Eng. Chem. Res.*, 2010, **49**, 2701-2706.
270. M. Shokrollahi Yancheshmeh, H. R. Radfarnia and M. C. Iliuta, *Journal of Natural Gas Science and Engineering*, 2016, **36**, 1062-1069.
271. S. D. Angeli, C. S. Martavaltzi and A. A. Lemonidou, *Fuel*, 2014, **127**, 62-69.
272. M. Zhao, M. Bilton, A. P. Brown, A. M. Cunliffe, E. Dvininov, V. Dupont, T. P. Comyn and S. J. Milne, *Energ. Fuel.*, 2014, **28**, 1275-1283.
273. L. Li, D. L. King, Z. Nie, X. S. Li and C. Howard, *Energ. Fuel.*, 2010, **24**, 3698-3703.
274. S. Wang, S. Yan, X. Ma and J. Gong, *Energy. Environ. Sci.*, 2011, **4**, 3805-3819.
275. Y. Li, C. Zhao, H. Chen, L. Duan and X. Chen, *Fuel*, 2010, **89**, 642-649.
276. V. Manovic and E. J. Anthony, *Energ. Fuel.*, 2009, **23**, 4797-4804.
277. P. T. Clough, M. E. Boot-Handford, M. Zhao and P. S. Fennell, *Fuel*, 2016, **186**, 708-713.
278. B. Balasubramanian, A. Lopez Ortiz, S. Kaytakoglu and D. P. Harrison, *Chem. Eng. Sci.*, 1999, **54**, 3543-3552.
279. R. Filitz, A. M. Kierzkowska, M. Broda and C. R. Müller, *Environ. Sci. Technol.*, 2012, **46**, 559-565.
280. V. Manovic, E. J. Anthony, G. Grasa and J. C. Abanades, *Energ. Fuel.*, 2008, **22**, 3258-3264.
281. L. He, H. Berntsen and D. Chen, *The Journal of Physical Chemistry A*, 2010, **114**, 3834-3844.
282. P. Pimenidou, G. Rickett, V. Dupont and M. V. Twigg, *Bioresour. Technol.*, 2010, **101**, 9279-9286.
283. A. Lopez Ortiz and D. P. Harrison, *Ind. Eng. Chem. Res.*, 2001, **40**, 5102-5109.
284. J. Fermoso, L. He and D. Chen, *Int. J. Hydrogen Energy*, 2012, **37**, 14047-14054.
285. Z.-s. Li, N.-s. Cai and J.-b. Yang, *Ind. Eng. Chem. Res.*, 2006, **45**, 8788-8793.
286. K. Johnsen, H. J. Ryu, J. R. Grace and C. J. Lim, *Chem. Eng. Sci.*, 2006, **61**, 1195-1202.
287. C. S. Martavaltzi, E. P. Pampaka, E. S. Korkakaki and A. A. Lemonidou, *Energ. Fuel.*, 2010, **24**, 2589-2595.
288. C. S. Martavaltzi and A. A. Lemonidou, *Chem. Eng. Sci.*, 2010, **65**, 4134-4140.
289. N. Chanburanasiri, A. M. Ribeiro, A. E. Rodrigues, A. Arpornwichanop, N. Laosiripojana, P. Praserthdam and S. Assabumrungrat, *Ind. Eng. Chem. Res.*, 2011, **50**, 13662-13671.
290. H. Z. Feng, P. Q. Lan and S. F. Wu, *Int. J. Hydrogen Energy*, 2012, **37**, 14161-14166.
291. M. Broda, A. M. Kierzkowska, D. Baudouin, Q. Imtiaz, C. Copéret and C. R. Müller, *ACS Catalysis*, 2012, **2**, 1635-1646.
292. J.-N. Kim, C. H. Ko and K. B. Yi, *Int. J. Hydrogen Energy*, 2013, **38**, 6072-6078.
293. M. Broda, V. Manovic, Q. Imtiaz, A. M. Kierzkowska, E. J. Anthony and C. R. Müller, *Environ. Sci. Technol.*, 2013, **47**, 6007-6014.
294. L. Barelli, G. Bidini, A. Di Michele, F. Gallorini, C. Petrillo and F. Sacchetti, *Appl. Energ.*, 2014, **127**, 81-92.
295. P. Xu, M. Xie, Z. Cheng and Z. Zhou, *Ind. Eng. Chem. Res.*, 2013, **52**, 12161-12169.
296. M. Broda, A. M. Kierzkowska and C. R. Müller, *Chem. Eng. Technol.*, 2013, **36**, 1496-1502.
297. H. R. Radfarnia and M. C. Iliuta, *Chem. Eng. Sci.*, 2014, **109**, 212-219.
298. H. R. Radfarnia and M. C. Iliuta, *Chemical Engineering and Processing: Process Intensification*, 2014, **86**, 96-103.
299. X. Chen, L. Yang, Z. Zhou and Z. Cheng, *Chem. Eng. Sci.*, 2017, **163**, 114-122.
300. I. Aloisi, A. Di Giuliano, A. Di Carlo, P. U. Foscolo, C. Courson and K. Gallucci, *Chem. Eng. J.*, 2017, **314**, 570-582.
301. A. Di Giuliano, J. Girr, R. Massacesi, K. Gallucci and C. Courson, *Int. J. Hydrogen Energy*, 2017

302. P. Xu, Z. Zhou, C. Zhao and Z. Cheng, *Catal. Today*, 2016, **259, Part 2**, 347-353.
303. C. Zhao, Z. Zhou, Z. Cheng and X. Fang, *Appl. Catal. B-Environ*, 2016, **196**, 16-26.
304. J. Phromprasit, J. Powell, S. Wongsakulphasatch, W. Kiatkittipong, P. Bumroongsakulsawat and S. Assabumrungrat, *Chem. Eng. J.*, 2017, **313**, 1415-1425.
305. B. Jiang, B. Dou, K. Wang, C. Zhang, M. Li, H. Chen and Y. Xu, *Chem. Eng. J.*, 2017, **313**, 207-216.
306. A. Antzara, E. Heracleous and A. A. Lemonidou, *Appl. Energ.*, 2016, **180**, 457-471.
307. C. Dang, H. Yu, H. Wang, F. Peng and Y. Yang, *Chem. Eng. J.*, 2016, **286**, 329-338.
308. L. He, J. M. S. Parra, E. A. Blekkan and D. Chen, *Energy. Environ. Sci.*, 2010, **3**, 1046-1056.
309. B. Dou, V. Dupont, G. Rickett, N. Blakeman, P. T. Williams, H. Chen, Y. Ding and M. Ghadiri, *Bioresour. Technol.*, 2009, **100**, 3540-3547.
310. N. Sánchez, J. M. Encinar and J. F. González, *Ind. Eng. Chem. Res.*, 2016, **55**, 3736-3741.
311. B. Dou, B. Jiang, Y. Song, C. Zhang, C. Wang, H. Chen, B. Du and Y. Xu, *Fuel*, 2016, **166**, 340-346.
312. B. Dou, C. Wang, H. Chen, Y. Song and B. Xie, *Int. J. Hydrogen Energy*, 2013, **38**, 11902-11909.
313. M. V. Gil, J. Fermoso, C. Pevida, D. Chen and F. Rubiera, *Appl. Catal. B-Environ*, 2016, **184**, 64-76.
314. G. Esteban-Díez, M. V. Gil, C. Pevida, D. Chen and F. Rubiera, *Appl. Energ.*, 2016, **177**, 579-590.
315. D. Y. Aceves Olivas, M. R. Baray Guerrero, M. A. Escobedo Bretado, M. Marques da Silva Paula, J. Salinas Gutiérrez, V. Guzmán Velderrain, A. López Ortiz and V. Collins-Martínez, *Int. J. Hydrogen Energy*, 2014, **39**, 16595-16607.

316. M. Z. Memon, X. Zhao, V. S. Sikarwar, A. K. Vuppaladadiyam, S. J. Milne, A. P. Brown, J. Li and M. Zhao, *Environ. Sci. Technol.*, 2017, **51**, 12-27.
317. K. D. Dewoolkar and P. D. Vaidya, *Energ. Fuel.*, 2015, **29**, 3870-3878.
318. Y. Ding and E. Alpay, *Chem. Eng. Sci.*, 2000, **55**, 3929-3940.
319. E. R. van Selow, P. D. Cobden, R. W. van den Brink, J. R. Hufton and A. Wright, *Energy Procedia*, 2009, **1**, 689-696.
320. E. R. van Selow, P. D. Cobden, P. A. Verbraeken, J. R. Hufton and R. W. van den Brink, *Ind. Eng. Chem. Res.*, 2009, **48**, 4184-4193.
321. J. Wang, L. Huang, R. Yang, Z. Zhang, J. Wu, Y. Gao, Q. Wang, D. O'Hare and Z. Zhong, *Energy. Environ. Sci.*, 2014, **7**, 3478-3518.
322. Z. Yong, Mata and A. E. Rodrigues, *Ind. Eng. Chem. Res.*, 2001, **40**, 204-209.
323. R. Singh, M. K. Ram Reddy, S. Wilson, K. Joshi, J. C. Diniz da Costa and P. Webley, *Energy Procedia*, 2009, **1**, 623-630.
324. M. K. Ram Reddy, Z. P. Xu and J. C. Diniz da Costa, *Ind. Eng. Chem. Res.*, 2008, **47**, 2630-2635.
325. G. Ji, J. Motuzas, G. Birkett, S. Smart, K. Hooman and J. C. Diniz da Costa, *Int. J. Hydrogen Energy*, 2017, **42**, 7997-8005.
326. G. Ji, M. Z. Memon, H. Zhuo and M. Zhao, *Chem. Eng. J.*, 2017, **313**, 646-654.
327. F. Bamiduro, G. Ji, A. P. Brown, V. A. Dupont, M. Zhao and S. J. Milne, *ChemSusChem*, 2017.
328. H. Kim, H. D. Jang and M. Choi, *Chem. Eng. J.*, 2015, **280**, 132-137.
329. R. Quinn, R. J. Kitzhoffer, J. R. Hufton and T. C. Golden, *Ind. Eng. Chem. Res.*, 2012, **51**, 9320-9327.
330. Y. Pan, Y. Zhang, T. Zhou, B. Louis, D. O'Hare and Q. Wang, *Inorg. Chem.*, 2017, **56**, 7821-7834.
331. X. Chen, Z. Xiong, Y. Qin, B. Gong, C. Tian, Y. Zhao, J. Zhang and C. Zheng, *Int. J. Hydrogen Energy*, 2016, **41**, 13077-13085.
332. K. Essaki, T. Muramatsu and M. Kato, *Int. J. Hydrogen Energy*, 2008, **33**, 4555-4559.
333. T. Zhao, M. Rønning and D. Chen, *J Energy Chem*, 2013, **22**, 387-393.
334. P. Sánchez-Camacho, I. C. Romero-Ibarra and H. Pfeiffer, *J CO2 Util*, 2013, **3–4**, 14-20.
335. L. Martínez-dlCruz and H. Pfeiffer, *J. Solid State Chem.*, 2013, **204**, 298-304.
336. M. Z. Memon, G. Ji, J. Li and M. Zhao, *Ind. Eng. Chem. Res.*, 2017, **56**, 3223-3230.
337. N. Santiago-Torres, I. C. Romero-Ibarra and H. Pfeiffer, *Fuel Process. Technol.*, 2014, **120**, 34-39.
338. E. Ochoa-Fernández, C. Lacalle-Vilà, T. Zhao, M. Rønning and D. Chen, *Stud. Surf. Sci. Catal.*, 2007, **167**, 159-164.
339. H. K. Rusten, E. Ochoa-Fernández, D. Chen and H. A. Jakobsen, *Ind. Eng. Chem. Res.*, 2007, **46**, 4435-4443.
340. K. B. Yi and D. Ø. Eriksen, *Sep. Sci. Technol.*, 2006, **41**, 283-296.
341. G. Ji, M. Zhao and G. Wang, *Energy*, 2018, **147**, 884-895.
342. G. Barbieri, F. Scura, F. Lentini, G. De Luca and E. Drioli, *Sep. Purif. Technol.*, 2008, **61**, 217-224.
343. W.-H. Chen, T.-C. Hsieh and T. L. Jiang, *Energy Convers. Manage.*, 2008, **49**, 2801-2808.
344. H. Sakai, T. Nakajima, N. Yoshida and S. Kishimoto, *React. Kinet. Catal. Lett.*, 1982, **19**, 297-301.
345. S. Hara, K. Sakaki and N. Itoh, *Ind. Eng. Chem. Res.*, 1999, **38**, 4913-4918.
346. T. Osaki and T. Mori, *React. Kinet. Catal. Lett.*, 2006, **89**, 333-339.
347. G. He, Y. Mi, P. Lock Yue and G. Chen, *J Membrane Sci*, 1999, **153**, 243-258.
348. H. Takaba and S.-i. Nakao, *J Membrane Sci*, 2005, **249**, 83–88.
349. Z. Chen, F. Po, J. R. Grace, C. Jim Lim, S. Elnashaie, A. Mahecha-Botero, M. Rakib, Y. Shirasaki and I. Yasuda, *Chem. Eng. Sci.*, 2008, **63**, 170-182.
350. Y. Chen, A. Mahechabotero, C. J. Lim, J. R. Grace, J. Zhang, Y. Zhao and C. Zheng, *Ind. Eng. Chem. Res.*, 2014, **53**, 6230-6242.
351. M.-B. Andrés, T. Boyd, J. R. Grace, C. Jim Lim, A. Gulamhusein, B. Wan, H. Kurokawa and Y. Shirasaki, *Int. J. Hydrogen Energy*, 2011, **36**, 4038-4055.
352. F. R. García-García, M. León, S. Ordóñez and K. Li, *Catal. Today*, 2014, **236, Part A**, 57-63.
353. M. A. Soria, S. Tosti, A. Mendes and L. M. Madeira, *Fuel*, 2015, **159**, 854-863.
354. G. Ji, G. Wang, K. Hooman, S. Bhatia and J. Diniz da Costa, *Front. Chem. Sci. Eng.*, 2012, **6**, 3-12.
355. M. Coroneo, G. Montante and A. Paglianti, *Ind. Eng. Chem. Res.*, 2010, **49**, 9300-9309.
356. N. Mori, T. Nakamura, K.-i. Noda, O. Sakai, A. Takahashi, N. Ogawa, H. Sakai, Y. Iwamoto and T. Hattori, *Ind. Eng. Chem. Res.*, 2007, **46**, 1952-1958.
357. M. K. Koukou, N. Papayannakos and N. C. Markatos, *Chem. Eng. J.*, 2001, **83**, 95-105.
358. M. K. Koukou, N. Papayannakos, N. C. Markatos, M. Bracht and P. T. Alderliesten, *Chem. Eng. Res. Des.*, 1998, **76**, 911-920.
359. W.-H. Chen, W.-Z. Syu and C.-I. Hung, *Int. J. Hydrogen Energy*, 2011, **36**, 14734-14744.
360. M. K. Koukou, G. Chaloulou, N. Papayannakos and N. C. Markatos, *Int. J. Heat Mass Transfer*, 1997, **40**, 2407-2417.
361. W.-H. Chen, C.-W. Tsai, Y.-L. Lin, R.-Y. Chein and C.-T. Yu, *Fuel*, 2017, **199**, 358-371.
362. H. Lindborg and H. A. Jakobsen, *Ind. Eng. Chem. Res.*, 2009, **48**, 1332-1342.
363. J. Xie, W. Zhong, B. Jin, Y. Shao and Y. Huang, *Adv. Powder Technol.*, 2013, **24**, 382-392.
364. A. Di Carlo, E. Bocci, F. Zuccari and A. Dell'Era, *Ind. Eng. Chem. Res.*, 2010, **49**, 1561-1576.
365. Y. Wang, Z. Chao and H. A. Jakobsen, *Journal of Natural Gas Science and Engineering*, 2010, **2**, 105-113.
366. J. Meyer, J. Mastin and C. S. Pinilla, *Energy Procedia*, 2014, **63**, 6800-6814.
367. C. Hawthorne, N. Poboss, H. Dieter, A. Gredinger, M. Zieba and G. Scheffknecht, *Biomass Conversion and Biorefinery*, 2012, **2**, 217-227.
368. C. Pfeifer, B. Puchner and H. Hofbauer, *Journal*, 2007, **5**.

369. S. Müller, J. Fuchs, J. C. Schmid, F. Benedikt and H. Hofbauer, *Int. J. Hydrogen Energy*, 2017, **42**, 29694-29707.
370. ASCENT (C-Shift) project, http://www.ascentproject.eu/project_sections.php?id=3).
371. *Fuel Cells Bulletin*, 2005, **2005**, 5.
372. The Stepwise Project, http://www.stepwise.eu/home/).
373. M. Zhao, T. L. Church and A. T. Harris, *Appl. Catal. B-Environ*, 2011, **101**, 522-530.
374. G. Ji, X. Xu, H. Yang, X. Zhao, X. He and M. Zhao, *Environ. Sci. Technol.*, 2017, **51**, 11484-11492.
375. Y. Song, G. Ji, X. Zhao, X. He, X. Cui and M. Zhao, *Energ. Fuel.*, 2017, DOI: 10.1021/acs.energyfuels.7b02330.
376. J. Sunarso, S. Baumann, J. M. Serra, W. A. Meulenberg, S. Liu, Y. S. Lin and J. C. Diniz da Costa, *J Membrane Sci*, 2008, **320**, 13-41.

Enhanced hydrogen production from thermochemical processes

Ji, Guozhao

2018-07-24

Guozhao Ji, Joseph G. Yao, Peter T. Clough, et al., Enhanced hydrogen production from thermochemical processes. Energy and Environmental Science, Volume 11, Issue 10, 2018, pp. 2647-2672
https://doi.org/10.1039/C8EE01393D